JBC RESEARCH ARTICLE

Evolutionary duplication of the leishmanial adaptor protein α-SNAP plays a role in its pathogenicity

Received for publication, December 1, 2024, and in revised form, March 3, 2025 Published, Papers in Press, March 19, 2025,
https://doi.org/10.1016/j.jbc.2025.108427

Shankari Prasad Datta and Chinmoy Sankar Dey*

From the Kusuma School of Biological Sciences, Indian Institute of Technology-Delhi, New Delhi, India

Reviewed by members of the JBC Editorial Board. Edited by Ursula Jakob

Essential-gene duplication during evolution promotes specialized functions beyond the typical role. Our *in silico* study unveiled two α-SNAP paralogs in *Leishmania*, a crucial component that, along with NSF, triggers disassembly of the cis-SNARE complex, formed during vesicle fusion with target membranes. While multiple α-SNAPs are common in many flagellated protists, including the trypanosomatids, they are unusual among other eukaryotes. This study explores the evolutionary and functional relevance of α-SNAP gene duplication in *Leishmania donovani*, emphasizing both subfunctionalization and neofunctionalization. We discovered that *L. donovani* α-SNAP (*Ld*α-SNAP) genes are transcribed in promastigote and amastigote stages, indicating they are not pseudogenes. Although the two paralogs share essential residues and structural features, only *Ld*α-SNAP$_{1660}$ (*Ld*α-SNAP1) can effectively substitute the function of its yeast counterpart, while *Ld*α-SNAP$_{3040}$ (*Ld*α-SNAP2) cannot. This functional difference is attributed to a replacement of alanine with phosphorylatable-serine in *Ld*α-SNAP1 during evolution from the most common ancestral ortholog. This modification is rarely observed in corresponding orthologs of other trypanosomatids. Incidentally, *Ld*α-SNAP paralogs exhibit differential localization in the ER and flagellar pocket. However, both paralogs, either actively or passively, regulate the secretion of exosomes and PM blebs, containing the virulence protein GP63. This indicates functional division and their indirect participation in the host's macrophage inactivation. Moreover, a small fraction of *Ld*α-SNAP1's presence in the flagellum hints at a potential role in sensing environmental cues and aiding the parasite's attachment to the sandfly's hindgut. Our findings underscore that duplicated *Ld*α-SNAPs have retained ancestral functions through subfunctionalization, and subsequently, they acquired parasite-specific neofunction(s) through the accumulation of natural mutation(s).

Leishmania, the etiological agent for leishmaniasis, has a digenetic life cycle involving an insect vector (*i.e.*, phlebotomine sandfly) and a vertebrate host. The disease manifests through the transition between two life stages: elongated, motile promastigotes in the sandfly gut and ovoid, non-motile amastigotes located within mammalian macrophages. The switching of the parasite from promastigotes to amastigotes within the vertebrate hosts disrupts the host's immune system, aiding the parasite's survival and proliferation (1, 2). When *Leishmania* promastigotes enter a mammalian host through the bite of an infected sand fly, they communicate with the host's macrophages by secreting virulence proteins (3). Some of these proteins are made or modified in the endoplasmic reticulum (ER) (4, 5). The promastigotes employ a conventional vesicle-mediated secretory pathway to transport these virulence proteins from ER into the extracellular milieu. This process involves the simultaneous release of exosomes-like extracellular microvesicles from the flagellar pocket (FP) and the blebbing of the plasma membrane (PM Blebs) from the cell surface (5, 6). Therefore, a well-developed vesicular trafficking system is crucial for this parasite to modulate macrophage signaling, breach the host immune barrier, and ensure its survival and propagation within the host, thereby establishing a persistent infection.

The precise targeting of vesicles to their designated destination and their subsequent fusion with the target membrane is regulated by the cytoplasmic proteins, N-ethylmaleimide-sensitive factor (NSF), and its adaptor α-Soluble NSF Attachment Protein (α-SNAP) (7–9). The α-SNAP is a ubiquitously expressed isoform of SNAP amongst three identified isoforms α, β, and γ in higher eukaryotes (10, 11). *In-silico* analysis revealed only α and γ-SNAP are present in the parasite genome, where β-SNAP has not been identified (12–14). Of these two isoforms, γ-SNAP interacts directly with NSF but does not bind to SNAP REceptors (SNAREs) (15). In contrast, α-SNAP can interact with both NSF and SNARE, playing a fundamental role in promoting the fusion of vesicle membranes with those of appropriate target compartments to form a continuous bilayer. α-SNAP accomplishes this by recruiting ATP-bound, ring-shaped, homo-hexameric NSF to the fused membrane after being bound directly to newly formed cis-SNARE complexes on the acceptor membrane (16). The positively charged residues on the concave face of α-SNAP electrostatically interact with the negatively charged residues on the convex face of SNAREs, forming an α-SNAP-cis-SNARE complex (17). A bound α-SNAP serves as an adaptor for NSF, as NSF itself lacks a direct binding site for SNAREs (18). During membrane fusion, the sequential recruitment of α-SNAP and NSF to the cis-SNARE bundle forms a large hetero-oligomeric complex called the 20S complex (19).

* For correspondence: Chinmoy Sankar Dey, csdey@bioschool.iitd.ac.in.

α-SNAP then stimulates the ATPase activity of NSF (16, 20). The activated NSF functions as a SNARE chaperone, utilizing energy from ATP hydrolysis to dissociate the 20S complex during subsequent membrane fusion reactions (21, 22). Therefore, α-SNAP appears to be a key component of the intracellular membrane fusion machinery.

Apart from its canonical functions in ER to Golgi trafficking, endosomal fusion, and exocytosis, α-SNAP is also well-known for various non-canonical, NSF-SNARE-independent functions. These include secretory organelle biogenesis, store-operated Ca^{2+} ion channel opening, inhibition of AMPK signaling to reduce mitochondrial biogenesis, cell-matrix adhesion, folliculogenesis, *etc.* (23–29). The number of α-SNAP genes varies among closely and distantly related eukaryotic lineages. For instance, the *Leishmania major* genome codes two paralogs of α/β-SNAP and one orthologue of γ-SNAP (14). Our BLAST search revealed that among these two isoforms, α and γ, α-SNAP is present in multiple copies in all kinetoplastids (*e.g.*, *Leishmania*, *Trypanosoma*, *etc.*). In contrast, opisthokonts contain only one copy (12, 14, 30). The presence of multiple paralogs of α-SNAP in the *Leishmania* genome is not unique; many flagellated parasites (*e.g.*, *Trichomonas*, *Giardia*, *etc.*) and some plants (*e.g.*, *Arabidopsis*, Soybean, *etc.*) exhibit this characteristic as well (12, 31, 32). Conversely, with a few exceptions within the taxa of Amoebozoa and Alveolate, most non-flagellates (*e.g.*, *Entamoeba*, *Toxoplasma*, *etc.*), fungi (*e.g.*, *Saccharomyces*, *Neurospora*, *etc.*), as well as certain insects (like *Drosophila*) and Metazoan (*e.g.* Human, mouse, *etc.*) generally contain a single α-SNAP, which drives their intracellular vesicular trafficking (13, 23, 27, 33–35).

The accessibility of complete genome sequence followed by genome-wide analysis of the eukaryotic pathogen database has enabled us to identify multiple paralogs of α-SNAP in most flagellated parasites, including the trypanosomatid *Leishmania*. The presence of multiple genes for the same protein in unicellular protists contradicts the widely held notion that eukaryotic lineages typically possess only a single α-SNAP ortholog. Our present study elucidates the significance of the unusual expansion of the number of α-SNAP genes in kinetoplastid *Leishmania* by structurally and functionally characterizing its two paralogs.

Results

The genome of Leishmania donovani *encodes two α-SNAP paralogs with structural features similar to canonical α-SNAP, both of which are transcribed throughout the parasite's life cycle*

Except for a few organisms, most eukaryotic genomes typically contain a single α-SNAP gene, but in a study of 47 protist genomes, multiple α-SNAP paralogs were identified, including two α/β-SNAPs in *L. major* as SNARE-interacting orthologs (12, 14, 30). Our independent BLAST search in the Eukaryotic Pathogen Genomic Database (vEuPathDB), using a well-characterized yeast/*Saccharomyces cerevisiae* α-SNAP (*Sc*Sec17), revealed multiple paralogs of α-SNAP in trypanosomatids and other flagellated protists. In contrast, most aflagellates possess a single copy of the gene (12). The integrated genomic database TriTrypDB annotates these identified leishmanial paralogs as putative SNAPs with Open Reading Frame (ORF) Ids LdBPK.20.2.001660 and LdBPK.32.2.003040, located on chromosomes 20 and 32, respectively. Moreover, reverse BLAST searches with individual putative *L. donovani* α-SNAP (*Ld*α-SNAP) sequences also identified α-SNAP orthologs from diverse taxonomic groups. A sequence comparison of α-SNAP orthologs across eukaryotes revealed that both putative *Ld*α-SNAP1 and *Ld*α-SNAP2 shared a high sequence identity of 49.6% and 41.5% with their closely related trypanosomatid's orthologs, *Trypanosoma brucei* $\alpha\text{-SNAP}_{3110}$ and $\alpha\text{-SNAP}_{7740}$, respectively (Table 1). In contrast, the sequence identity with the α-SNAPs of apicomplexan parasite *Toxoplasma gondii* and diplomonads *Giardia lamblia* was notably low (Table 1). Although mammals exhibit a high sequence identity of 98% between humans and mice, other eukaryotic α-SNAP orthologs tend to share relatively low to moderate identity values ranging from 22% to 39%. This suggests that the identified leishmanial ORFs are indeed α-SNAP orthologs in this parasite. To further validate our findings, we analyzed the sequences of the putative *Ld*α-SNAPs for considerable conservation of domain(s), key secondary structural elements, and essential amino acids. The Pfam analysis indicated that, like other eukaryotic orthologs, the proteins translated from ORF LdBPK.20.2.001660 (encodes *Ld*α-SNAP1) and LdBPK.32.2.003040 (encodes *Ld*α-SNAP2) are single-domain proteins containing a SNAP domain, a characteristic feature of eukaryotic α-SNAP (Fig. 1*A*). Thus, the presence of the SNAP domain in these putative *Ld*α-SNAPs strongly supports the arguments that they are, indeed, α-SNAP orthologs in this parasite.

While the SNAP domain is evolutionary conserved, its size often varies within or across the eukaryotic taxa. Notably, the two *Ld*α-SNAPs exhibit some discrepancy in SNAP domain size: *Ld*α-SNAP1 and *Ld*α-SNAP2 possess shorter SNAP domains of 276 and 278 amino acids, respectively, compared to *Sc*Sec17 (282 amino acids), although their full-lengths are comparable (282 and 291 amino acids in *Leishmania* compared to 292 amino acids in yeast) (Fig. 1*A*). Furthermore, both *Ld*α-SNAPs exhibit conservation of the 14 α-helices when their secondary structures were predicted using the fold recognition-based modeling server I-TASSER (Fig. 1*B*). Interestingly, aside from minor differences in length, almost all the predicted α-helices of both *Ld*α-SNAPs closely align with the helices of the *Sc*Sec17 crystal structure (Fig. 1, *B* and *C*). Conservation was also observed in the N-terminal twisted sheet and C-terminal globular bundle, required for SNARE and NSF binding, respectively (36), when analyzing the predicted tertiary structures of *Ld*α-SNAPs, generated using the fold recognition method (Fig. 1*C*). The first nine α-helices in the predicted tertiary structure of both *Ld*α-SNAPs form a twisted sheet of α-helical hairpin, while the terminal five adopt an α-helical globular bundle-like conformation (Fig. 1*C*). The concave and convex surfaces are also present in the predicted models of both *Ld*α-SNAPs (Fig. S1). Therefore, the

Table 1
Pairwise sequence identities among α-SNAPs from diverse eukaryotic taxonomic group

1	2	3	4	5	6	7	8	9	10	11	12	13	14	15		
**	43.6	39.1	39.5	30.6	36.5	30.3	25.3	27.9	24.1	27.8	21.5	19.3	28.4	26.9	1	*O. sativa*
	**	36.8	36.8	30.5	33.0	28.0	22.2	27.2	22.6	34.0	24.3	18.0	26.8	23.5	2	*C. reinhardtii*
		**	98.0	34.1	34.7	30.6	25.9	26.1	23.7	26.9	23.9	20.8	26.2	26.7	3	*H. sapiens*
			**	34.1	34.7	31.2	26.6	26.5	24.0	27.2	24.2	21.8	26.2	27.4	4	*M. musculus*
				**	40.5	25.4	19.8	23.3	23.7	25.6	19.7	21.1	25.2	23.4	5	*S. cerevisiae*
					**	28.1	27.5	26.7	22.9	23.3	24.0	19.9	25.7	23.6	6	*A. oryzae*
						**	23.1	22.6	20.9	25.1	22.6	20.1	20.0	21.7	7	*T. gondii*
							**	25.1	23.5	25.3	22.6	18.6	25.9	19.0	8	*E. histolytica*
								**	23.7	22.6	25.2	19.8	49.6	24.7	9	*T. brucei*_3110
									**	20.1	19.3	16.9	21.3	41.5	10	*T. brucei*_7740
										**	30.6	22.6	27.7	20.5	11	*G. lamblia*_17224
											**	21.6	21.7	18.0	12	*G. lamblia*_16521
												**	21.5	20.4	13	*G. lamblia*_10856
													**	23.6	14	*L. donovani*_α-SNAP1
														**	15	*L. donovani*_α-SNAP2

conservation of nearly all structural features, found in conventional α-SNAP, within leishmanial orthologs, suggests that they are likely functionally analogous to other eukaryotic α-SNAPs, participating in vesicular trafficking as a requisite linker between NSF and SNARE to form a stable 20S complex on the acceptor membrane.

Both identified leishmanial genes are paralogs of the common ancestral gene, α-SNAP. It is likely that both these genes are not transcribed simultaneously; one may experience a period of relaxed selection, which could indicate it is a pseudogene. Alternatively, the parasite might select these two copies for its two life-cycle stages and express them one at a time. To investigate this further, we qualitatively monitored the expression of two *Ld*α-SNAP genes (or their transcripts) during two major life cycle stages of *Leishmania*. We used reverse transcription PCR with cDNA (synthesized from total RNA extracted from both promastigotes and amastigotes) as templates, and gene-specific primers (listed in Table S1) to detect changes in gene expression. For housekeeping control, we measured the transcription of the 18S rRNA gene (amplicon length 197 bp) (Fig. 1*D*; Lane 1 and 2) and the gene for 40S ribosomal protein S8 (amplicon length 205 bp) (Fig. 1*D*; Lane 3 and 4) (37, 38). Each *Ld*α-SNAP gene-specific primer pair yielded highly specific amplicons: 245 bp corresponding to the *Ld*α-SNAP1 gene (Fig. 1*D*; Lane 5 and 6; Black arrows) and 152 bp corresponding to the *Ld*α-SNAP2 gene (Fig. 1*D*; Lane 7 and 8; White arrows) from cDNA collected from both life stages of *Leishmania*. Additionally, we monitored the expression of the Receptor adenylate cyclase-A (racA) gene (221 bp) (Fig. 1*D*; Lane 9 and 10) and the A2 gene (homologous to *Plasmodium* S antigen) (134 bp) (Fig. 1*D*; Lane 11 and 12). The racA gene is known to be transcribed only in the insect stage (promastigotes), while the A2 gene is transcribed in the mammalian host stage (amastigotes), serving as stage-specific controls (39–41). Overall, the results of our gene expression analysis indicate that the identified *Ld*α-SNAP orthologs are not pseudogenes and are transcribed throughout the life cycle of this protist. This suggests that their activity may be required at all stages of the parasite's life cycle.

Conservation of membrane and SNARE-interacting properties in Ldα*-SNAPs suggests their functional conservation in membrane trafficking as well*

The crystal structure of *Sc*Sec17 and the predicted structures of *Ld*α-SNAPs differ mainly by the presence of an extended α-helical patch (α1′) towards the N-terminal that connects helices α-1 and α-2 (Fig. 1*B*). This α-helical patch area adopts a small α-turn (α1′) called a membrane-interacting loop (MIL), comprising hydrophobic residues and serves as a site for membrane-attachment (42). Multiple sequence alignment (MSA) and predicted homology models revealed that the hydrophobic residues in the corresponding region of *Ld*α-SNAP1 and *Ld*α-SNAP2 form an unstructured loop/MIL (Fig. 1*C*, marked with dotted boxes; and Fig. 2*A*, region in between α1 and α2). Two highly conserved, exposed, hydrophobic residues in this MIL likely embed into the membrane lipid bilayer, contributing stability to the 20S complex on the acceptor membrane (42). Our MSA demonstrates that these two hydrophobic residues are conserved in the corresponding unstructured region of both *Ld*α-SNAPs (Fig. 2*A*, marked with a black box and asterisks). Specifically, *Ld*α-SNAP1 has two consecutive phenylalanine (F19 and F20), while *Ld*α-SNAP2 contains tryptophan (W21) and phenylalanine (F22) in this unstructured region (Fig. 2*A*, marked with a black box and asterisks), which is consistent with the pattern observed in other eukaryotes. Existing literature has shown that mutation of two highly conserved hydrophobic residues (F27 and F28) in the MIL of bovine α-SNAP to the polar amino acid serine prevents SNARE disassembly on liposome membranes (42). Therefore, the presence of two consecutive phenylalanine (F19 and F20) and the combination of tryptophan (W21) and phenylalanine (F22) in the MIL of *Ld*α-SNAP1 and *Ld*α-SNAP2, respectively, suggests that these paralogs may play a role in the disassembly of the membrane-bound cis-SNARE complex. The stoichiometry of the 20S complex is reported as 6:3:1 (NSF: α-SNAP: SNARE), and it is important to note that NSF does not interact directly with SNARE (43). To gain a better understanding of their role in cis-SNARE bundle disassembly, we next examined the SNARE interacting surfaces of these two leishmanial paralogs.

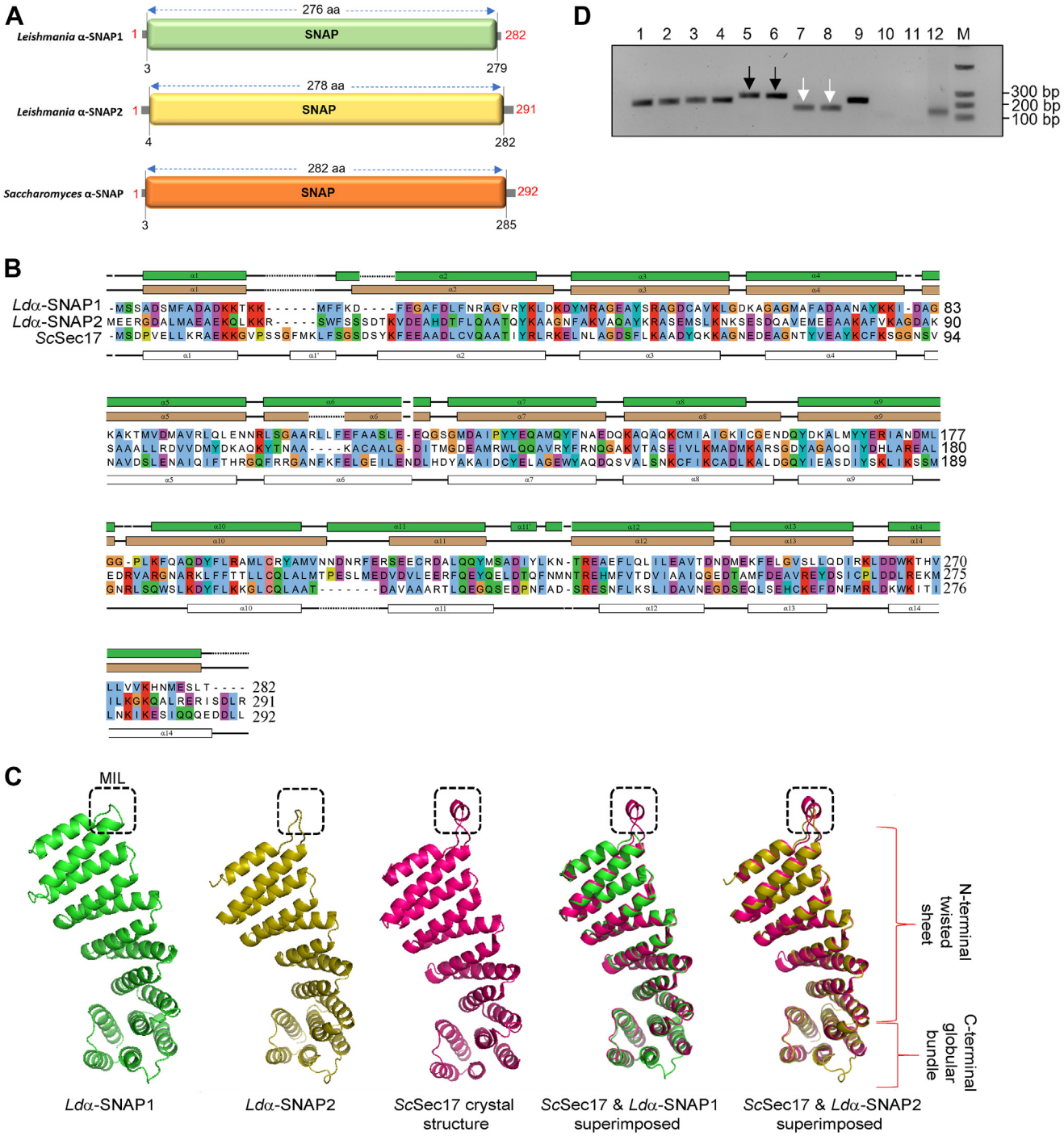

Figure 1. The domain architecture and secondary structural elements of putative *Ld*α-SNAP1 and *Ld*α-SNAP2, and the transcription of the genes encoding these proteins in promastigote and amastigote life forms of *Leishmania donovani*. *A*, diagrammatic representation of the architecture of the SNAP domain in identified putative α-SNAP orthologs of *Leishmania* and comparison of the SNAP domain boundaries of leishmanial SNAPs with yeast α-SNAP. *B*, the complete amino acid sequences of putative leishmanial α-SNAPs were aligned with well-documented *S. cerevisiae* α-SNAP ortholog Sec17. The region of amino acid sequences, within *Leishmania* SNAP paralogs, that are predicted to form an α-helix, have been marked with *colored boxes* (α-SNAP1- *Green* and α-SNAP2- fawn) above the alignment. The reported α-helices of the Sec17 crystal structure (PDB Id:1QQE) were represented with *white* boxes, having the helix number starting from α1 to α14, below the sequence alignment. The *solid lines* between the helices designate loop regions, and the *dashed lines* correspond to gaps in the alignment. *C*, predicted tertiary structure shows conservation of two principal domains *viz.* twisted sheet (formed by N-terminal nine α-helices) and globular bundle domain (formed by C-terminal five α-helices) within each leishmanial α-SNAP, just like yeast Sec17 crystal structure. The membrane-interacting sites/loop (MIL) of leishmanial and yeast α-SNAPs were marked with *black boxes*. *D*, qualitative analysis of the transcriptional gene expression or the presence of mRNA transcripts of the identified putative α-SNAP1 and α-SNAP2 in *Leishmania donovani* promastigotes and amastigotes was measured using reverse transcription PCR. The PCR amplification was carried out using gene-specific primers and the cDNA as a template, prepared from *L. donovani* promastigotes and amastigotes. Lanes 1,3,5,7,9 and 11 represent amplification using promastigote's cDNA, while lanes 2,4,6,8,10, and 12 show amplification of desired genes from amastigote's cDNA. The transcription of 18S rRNA (Lanes 1 and 2) and 40S ribosomal protein S8 (Lanes 3 and 4) were used as housekeeping control genes. The *black arrows* (Lanes 5 and 6) and white arrows (Lanes 7 and 8) marked the PCR amplified products corresponding to a small segment of the α-SNAP1 and α-SNAP2 genes, respectively. The transcriptional expressions of racA (Lanes 9 and 10) and A2 (Lanes 11 and 12) genes were used as stage-specific control for promastigotes and amastigotes, respectively. The M stands for DNA size marker.

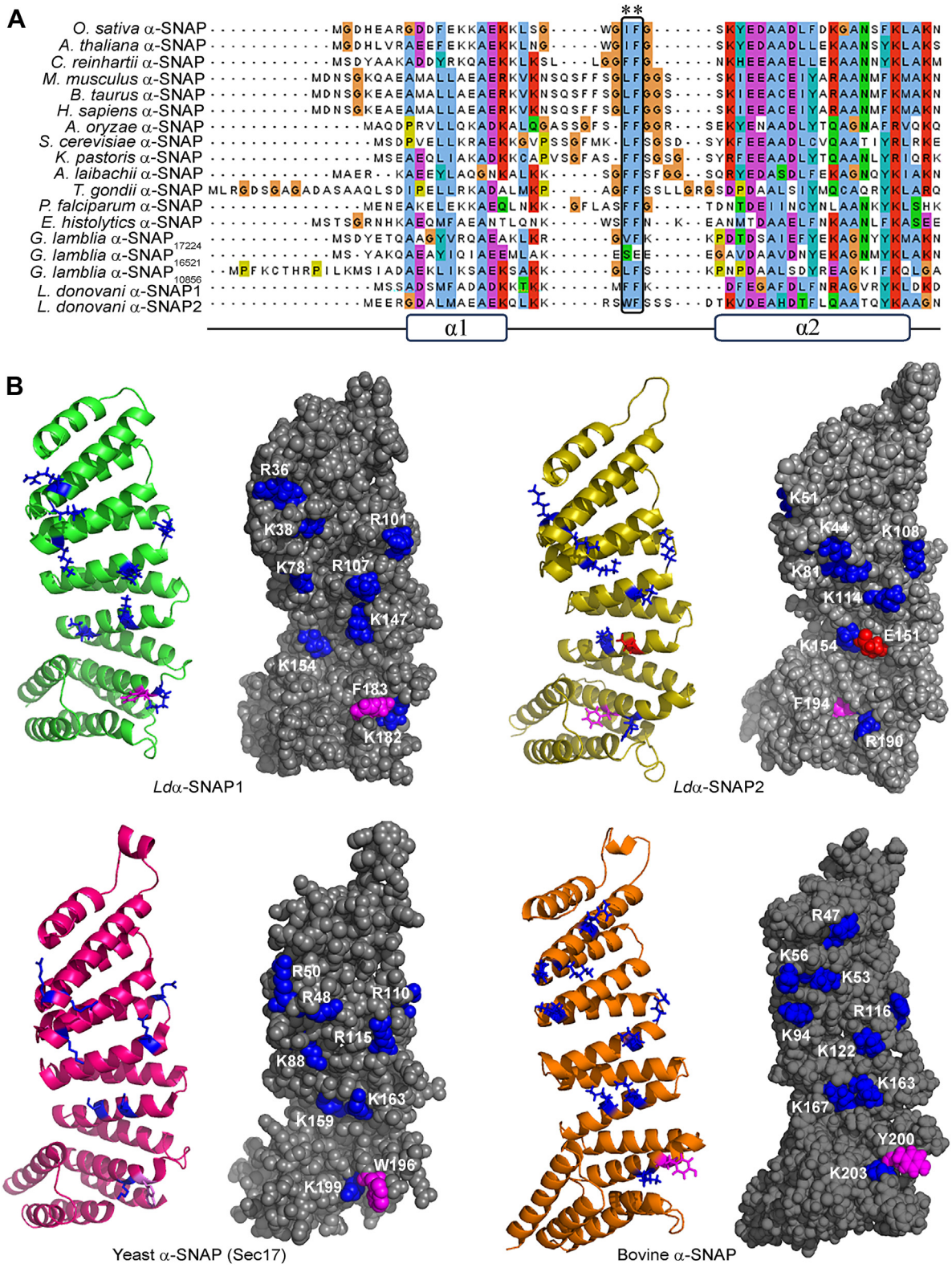

Figure 2. Membrane attachment site and SNARE-interacting surface of leishmanial α-SNAP paralogs. *A*, multiple sequence alignment of the N-terminal region of α-SNAP proteins from organisms belonging to different taxonomic groups indicates conservation of hydrophobic loop or membrane-interacting loop (MIL) between helix α1 and α2, that were previously shown to be involved in interaction with membrane lipids. The *red box* and *asterisks* point out the presence of two highly conserved hydrophobic residues within the MIL of all eukaryotic α-SNAPs, including the leishmanial orthologs. *B*, in the concave face of *Ldα*-SNAPs, the amino acid residues that carry a net positive charge and an aromatic residue, which are likely to participate in SNARE-binding, were marked in both the 3D space-filling and threading models with *blue* and *magenta colored spheres and sticks*, respectively. The only negatively charged residue in the space-filling and threading models of *Ldα*-SNAP2 was represented with *red-colored spheres and sticks*. Similarly, the essential positively charged and aromatic residues at the concave face of *Saccharomyces cerevisiae* and *Bos taurus* α-SNAPs, which were previously reported to be

The concave face of the N-terminal twisted sheet of α-SNAP interacts with SNAREs through electrostatic interaction between its basic residues and the acidic residues located on the convex face of the SNARE complex (17). Homology models of *Ld*α-SNAP1 and *Ld*α-SNAP2 reveal a similar charge distribution on the corresponding surfaces, which contains a combination of basic and aromatic residues (Fig. 2*B*, marked with colored spheres and sticks and Table S2). When comparing the positions of these basic residues with those in yeast and bovine α-SNAPs, we observed some differences: i) In *Ld*α-SNAPs, a basic residue (K182 in *Ld*α-SNAP1 and R190 in *Ld*α-SNAP2) precedes an aromatic residue (F183 in *Ld*α-SNAP1 and F194 in *Ld*α-SNAP2), whereas the order is reversed in yeast (W196, K199) and bovine (Y200, K203) α-SNAPs, ii) A lysine residue (K51) in *Ld*α-SNAP2 was shifted towards the edge of the concave face compared to the front face position of corresponding basic residues in yeast (R50) and bovine (K56) α-SNAPs, iii) An arginine (R101) and a lysine (K108) residue in *Ld*α-SNAP1 and *Ld*α-SNAP2, respectively, were shifted to the front face compared to the corresponding arginine residues in yeast (R110) and bovine (R116) α-SNAPs, positioned at the edge. Furthermore, a basic residue, present in yeast (K163) and bovine (K163) α-SNAPs as well as *Ld*α-SNAP1 (K147), has been replaced by acidic glutamate (E151) in *Ld*α-SNAP2, indicating a charge inversion (Fig. 2*B*). Despite these discrepancies in the distribution of charged residues on the potential SNARE-interacting surface of *Ld*α-SNAPs, the conservation of the basic residues and an aromatic residue on this surface, similar to yeast and bovine SNAPs, suggests that *Ld*α-SNAPs may retain SNARE-interacting properties. Given that both membrane-binding and SNARE interacting attributes are present in *Ld*α-SNAPs, it is likely that these paralogs functionally resemble their eukaryotic orthologs.

Only one of the Ldα*-SNAP genes encodes a protein that is functionally analogous to* Sc*Sec17*

To functionally characterize the *Ld*α-SNAPs, we could not use gene knockout in *Leishmania* because α-SNAP is essential for the organism's viability (44, 45). Instead, we employed a yeast model, which allows for easier genetic manipulation. We conducted a yeast-based functional complementation assay to test whether structural similarities between the *Sc*Sec17 and *Ld*α-SNAPs result in functional conservation. Cross-species functional complementation was performed using a yeast conditional mutant strain RSY269. This strain contains a mutation in the chromosomal *SEC17* gene (*sec17–1* allele) and thereby induces conditional lethality, *i.e.*, it allows yeast cells to grow at 30 °C but restricts its growth at 37 °C (46). We then assessed whether the *Ld*α-SNAPs could revert the mutant phenotype of RSY269 to its wild-type phenotype. Toward this, we introduced and expressed the *Ld*α-SNAPs individually into the RSY269 strain. The episomal expression of wild-type *Sc*Sec17 and the empty plasmid backbone served as positive and negative controls, respectively. The transformants carrying *Ld*α-SNAPs, *ScSEC17*, and empty vector all showed comparable growth at the permissive temperature of 30 °C, with no observable growth defect among them (Fig. 3*A*). However, we found that one of the *Ld*α-SNAPs, *Ld*α-SNAP1, was able to restore normal growth at the nonpermissive temperature of 37 °C, similar to positive control. In contrast, *Ld*α-SNAP2, was unable to rescue the growth defect at 37 °C and the resulting strain failed to grow on synthetic media lacking uracil (Fig. 3*A*). These results indicate that despite having all the structural features of a conventional α-SNAP, the two *Ld*α-SNAP paralogs exhibit divergence in their ability to complement the function of *Sc*Sec17. Specifically, *Ld*α-SNAP1 appears to be functionally analogous to *Sc*Sec17, while *Ld*α-SNAP2 may have undergone parasite-specific changes to fulfill a distinct role within *Leishmania*.

A phosphorylatable-serine or glutamate at position six is essential for α-SNAP function

Multiple paralogs can emerge from a common ancestral gene through duplication and may vary in sequences or structure. Even a single nucleotide substitution during gene duplication can significantly impact protein function (47–49). Notably, despite the conserved SNAP domain and overlapping secondary structural elements, *Ld*α-SNAP paralogs exhibit only 23% sequence identity between them. This disparity led us to hypothesize that the substitution of essential amino acid(s) could be a potential reason for the inability of *Ld*α-SNAP2 to substitute the *Sc*Sec17 functionally in the cross-species complementation experiment.

A previous report has shown that *T. gondii*'s α-SNAP (*Tg*α-SNAP) is phosphorylated on a serine residue at position 6 toward its N-terminal. This post-translational modification regulates secretory traffic and apicomplexan-specific organelle biogenesis within this parasite (23). Considering that *Leishmania* and *Toxoplasma* are obligate intracellular parasites of vertebrates, we search for the presence of serine residue towards the N-terminal region of leishmanial α-SNAPs (especially at the sixth position of the proteins). We have aligned the sequences of *Tg*α-SNAP and *Ld*α-SNAPs with a pairwise sequence alignment tool. Our sequence alignment revealed that the serine at position six is conserved only in *Ld*α-SNAP1 (Fig. 3*B*, marked with a black box and asterisk). Meanwhile, *Ld*α-SNAP2 contains an aspartate residue at this position (Fig. 3*B*, marked with red box). The conservation of serine-6 is also observed in one of the α-SNAP paralogs across different strains of *L. donovani* and diverse *Leishmania* species (Fig. S2, *A* and *B*, marked with red boxes). Similar to *Tg*α-SNAP, we speculate that the serine-6 in *Ld*α-SNAP1 is also important for its functionality. Conversely, the presence of aspartate, in place of serine, in *Ld*α-SNAP2 might be the substitution underpinning the deviation in its functional site compared to that of *Ld*α-SNAP1. We next sought to determine the

involved in SNARE-interaction, were highlighted in their corresponding space-filling and threading models with similarly *colored spheres and sticks*, as mentioned above. The positions of the predicted SNARE-interacting amino acids of leishmanial paralogs were then compared with the corresponding well-documented residues of yeast and bovine α-SNAP orthologs.

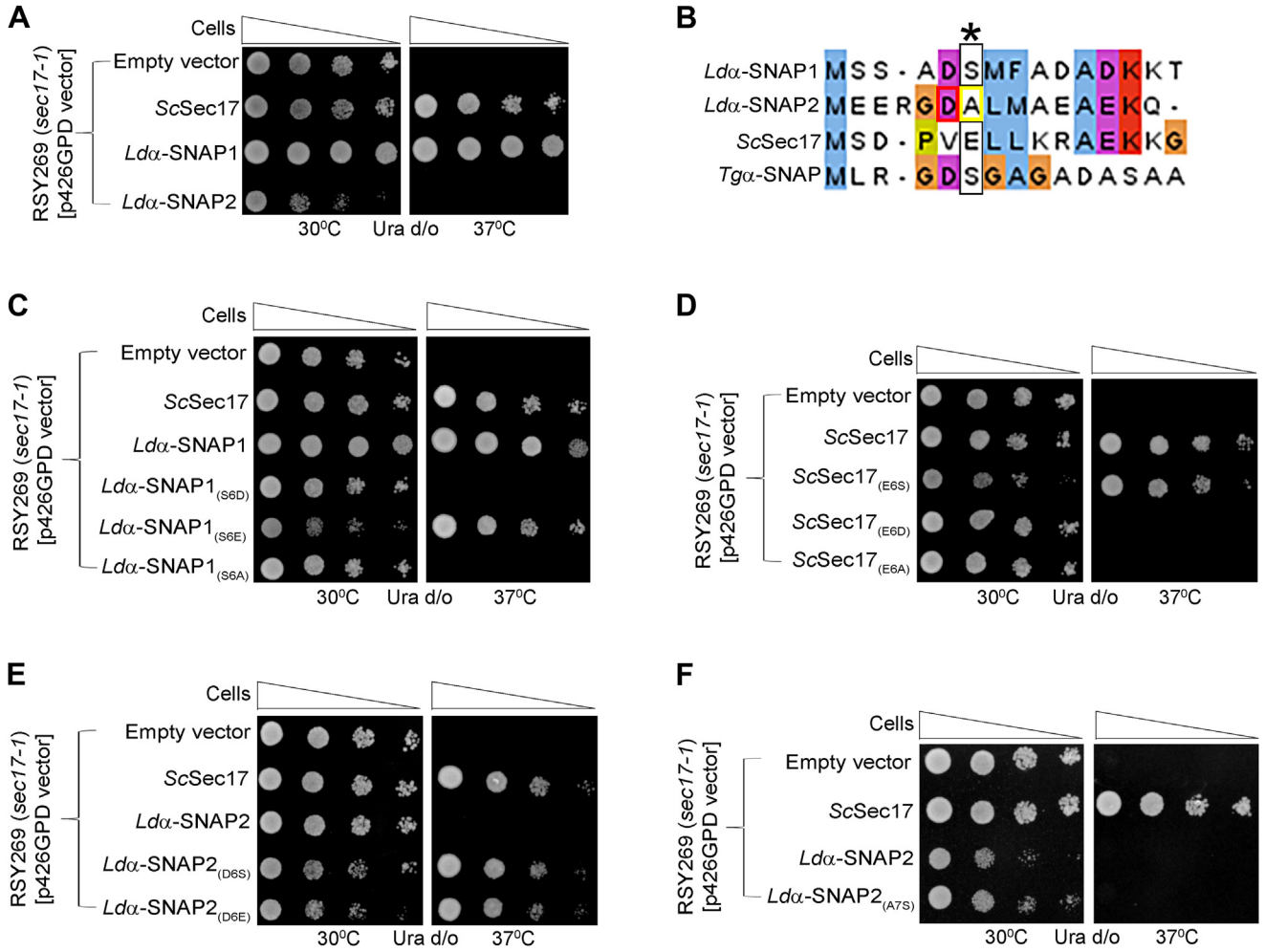

Figure 3. Functional complementation of *L. donovani* putative α-SNAPs in yeast *sec17–1* mutant strain and the critical role of an N-terminally located phosphorylatable-serine/glutamate in the functionality of α-SNAP. *A*, both leishmanial α-SNAPs, α-SNAP1, and α-SNAP2, were tested for their abilities to functionally substitute yeast α-SNAP Sec17 within temperature-sensitive *sec17-1* mutant yeast strain RSY269. The mutant yeast cells were transformed with the constructs p426GPD-*Ld*α-SNAP1, p426GPD-*Ld*α-SNAP2, p426GPD-*SEC17* (positive control), and empty p426GPD vector (negative control). The transformants were spotted on yeast synthetic medium lacking uracil (Ura d/o) plates. Subsequently, their growth was monitored at permissive (30 °C) and nonpermissive temperatures (37 °C) for 2 days. *B*, multiple sequence alignment of N-terminal 15 amino acids of *Leishmania*, yeast, and *Toxoplasma* α-SNAP orthologs to search for the well-defined phosphorylatable-serine residue in α-SNAP paralogs of trypanosomatid parasite *Leishmania donovani*. The *black box* and *asterisk* indicate conserved phosphorylatable-serine/glutamate residue at the sixth position of proteins. The *red* box represents the substitution of conserved serine/glutamate with aspartate at the sixth position of *Ld*α-SNAP2. The *yellow box* shows alanine-7 of *Ld*α-SNAP2 aligned with conserved serine-6/glutamate-6 in multiple sequence alignment. Cross-species complementation in yeast hypomorph using the phosphomimetic, phosphorylatable, non-phosphorylatable, and similarly charged residue substituted α-SNAP mutants. Constructs containing: *C*, the wild-type α-SNAP1, phosphomimetic: α-SNAP1$_{(S6D)}$, α-SNAP1$_{(S6E)}$ and non-phosphorylatable: α-SNAP1$_{(S6A)}$ substitution mutants, *D*, the wild-type Sec17 and its mutants: Glutamate$_6$Serine, Glutamate$_6$Aspartate and Glutamate$_6$Alanine, *E*, the wild-type α-SNAP2, phosphorylatable α-SNAP2$_{(D6S)}$, and a very similar negatively charge substituted *i.e.* α-SNAP1$_{(D6E)}$ mutant, and. *F*, phosphorylatable α-SNAP2$_{(A7S)}$ mutants, were individually transformed in temperature-sensitive yeast strain RSY269. Growth of these transformants at both permissive (30 °C) and nonpermissive temperature (37 °C) was assessed by spotting serial dilutions on yeast synthetic medium lacking uracil (Ura d/o).

phosphorylation prediction score for the identified serine-6 of *Ld*α-SNAP1. Our analysis revealed a score of 0.958, which is significantly higher than the threshold value of 0.500 and comparable to the prediction score of 0.984 for serine-6 of *Tg*α-SNAP (Table S3). Since *Ld*α-SNAP1 tested positive in the functional complementation assay while *Ld*α-SNAP2 did not, we anticipated that serine would be conserved in *Sc*Sec17 towards its N-terminal. Surprisingly, our MSA of *Ld*α-SNAPs with *Sc*Sec17 revealed that position six in *Sc*Sec17 contains glutamate instead of serine (Fig. 3*B*, marked with a black box and asterisk). Notably, a previous report demonstrated that substituting glutamic acid for serine in bovine prolactin mimics the phosphorylation, and the mutated protein exhibits biological activity similar to that of wild-type protein (50). These findings provide valuable insights into the possible phosphorylation of serine-6 in *Ld*α-SNAP1.

To investigate the impact of phosphorylation at the targeted serine-6 residue of *Ld*α-SNAP1, as well as the effect of phosphomimetic substitution (glutamate or aspartate in place of the phosphorylatable-serine) on the functionality of this protein, we conducted functional complementation experiments in RSY269. In these experiments, we used phosphomimetic

mutants (S6D and S6E) along with non-phosphorylatable mutants (S6A) of α-SNAP1. Our data indicated that the overexpression of the phosphomimetic α-SNAP1$_{(S6D)}$ and non-phosphorylatable α-SNAP1$_{(S6A)}$ mutants had a deleterious effect, completely inhibiting the growth of RSY269 at 37 °C (Fig. 3*C*). Surprisingly, the phosphomimetic serine-6 to glutamate exchange in α-SNAP1 facilitated the growth of RSY269 similar to wild-type (Fig. 3*C*). We observed similar growth pattern of RSY269 expressing both wild-type and mutant *Sc*Sec17. Additionally, our study demonstrated that replacing the glutamate at position six of *Sc*Sec17 with aspartate or alanine impaired protein functionality, leading to complete inhibition of RSY269 proliferation at 37 °C (Fig. 3*D*). Notably, RSY269, expressing mutant Sec17$_{(E6S)}$, grew at a rate similar to the wild-type at 37 °C (Fig. 3*D*). We then calculated the phosphorylation prediction score for serine after substituting glutamate with serine at position six of *Sc*Sec17, which yielded a score of 0.518, exceeding the threshold value of 0.500 (Table S3). We also analyzed *Ld*α-SNAP2, which lacks any serine or glutamate residue at its sixth position (Fig. 3*B*, marked with red box) and therefore cannot complement the function of *Sc*Sec17 (Fig. 3*A*). To determine the impact of replacing the aspartate-6 of *Ld*α-SNAP2 with the similarly charged glutamate, and polar, uncharged serine (which had a phosphorylation prediction score of 0.976), we screened for gain-of-function in the functional complementation experiment. Our results undeniably showed that these amino acid substitutions in *Ld*α-SNAP2 significantly improved protein functionality, specifically, *Ld*α-SNAP2$_{(D6S)}$ and *Ld*α-SNAP2$_{(D6E)}$ mutants functionally complemented *Sc*Sec17, unlike the wild-type *Ld*α-SNAP2 (Fig. 3*E*). However, we cannot rule out the presence of alanine (alanine-7) in *Ld*α-SNAP2, which aligned with the serine-6 of *Ld*α-SNAP1 and glutamate-6 of *Sc*Sec17 in our MSA (Fig. 3*B*, marked with a yellow box). We, therefore, replaced the alanine-7 residue of *Ld*α-SNAP2 with serine through site-specific mutation. We subsequently calculated the phosphorylation prediction score for serine-7 (after alanine-7 to serine substitution in *Ld*α-SNAP2), resulting in a score of 0.958, significantly higher than the threshold value of 0.500. Despite the high phosphorylation score for serine-7, the *Ld*α-SNAP2$_{(A7S)}$ mutant failed to complement *Sc*Sec17 in the complementation study (Fig. 3*F*). This outcome clearly highlights the importance of the position of the serine or glutamate residue in the functionality of α-SNAP. Therefore, our functional complementation study identified phosphorylatable-serine or glutamate residue, particularly at position 6, as the most influencing residue for the proper functioning of α-SNAP. Our findings suggest that similar to the *Tg*α-SNAP, the phosphorylatable serine at the sixth position is also essential for the functionality of *Ld*α-SNAP1. However, the absence of this phosphorylatable-serine at position six of *Ld*α-SNAP2 suggests that its functionality may not rely on this serine residue. Furthermore, our study illustrates an example of amino acid substitution during gene duplication, with the presence of aspartate instead of serine at the sixth position of *Ld*α-SNAP2, potentially contributing to a change in functional specificity compared to *Ld*α-SNAP1.

Two Leishmania *α-SNAPs showing non-overlapping distributions within promastigotes*

Our functional complementation in yeast hypomorphs indicates that the identified leishmanial paralogs are not functionally analogous. This suggests that the duplication of the α-SNAP gene in *Leishmania* may be due to the need for these proteins to function at distinct cellular locations or compartments within this parasite. We then monitored their subcellular distribution to understand the reason behind such functional divergence between these two *Ld*α-SNAPs. We have used a custom-made polyclonal antibody against *Ld*α-SNAP1 and episomally expressed the GFP-fused *Ld*α-SNAP2 protein for subcellular localization study. The specificity of the anti-*Ld*α-SNAP1 antibody was assessed by western immunoblotting (WB) with wild-type *L. donovani* cell lysates. The full-length blots displayed the expected prominent band of ∼31 kDa (Fig. S3). Since *Ld*α-SNAP1 and *Ld*α-SNAP2 are orthologs of the α-SNAP, there was a possibility that the antibody for full-length *Ld*α-SNAP1 could crosstalk with *Ld*α-SNAP2. Therefore, we first analyzed and compared the antigenic regions of both *Ld*α-SNAPs. Despite their orthologous/paralogous relationship, we found complete dissimilarities in both molecular regions and the lengths of their respective epitopes (Table S4). Hence, in WB, the anti-α-SNAP1 antibody specifically recognized its corresponding endogenous *Ld*α-SNAP1 protein in whole-cell lysates of both untransfected and GFP-fused *Ld*α-SNAP2 transfected promastigotes (Fig. 4*A*). However, the anti-α-SNAP1 antibody failed to detect GFP-fused *Ld*α-SNAP2 in the lysates of promastigotes overexpressing GFP-fused *Ld*α-SNAP2. This construct was immunodetected by anti-GFP antibody (Fig. 4*A*). Based on these results, we conclude that the anti-α-SNAP1 antibody is inherently specific and binds exclusively to the epitopes present on the corresponding protein *Ld*α-SNAP1.

Next, the immunolocalization study on fixed transgenic promastigotes expressing GFP-fused *Ld*α-SNAP2 revealed a bright red fluorescence at the ER after immunolabelled with anti-GFP antibody and its corresponding Alexa Fluor 555 conjugated secondary antibody (Fig. 4*B*, upper panel, marked with white arrows). Meanwhile, the empty GFP was uniformly localized throughout the cytoplasm of fixed promastigotes (Fig. 4*B*, lower panel). The ER localization of *Ld*α-SNAP2 in live promastigotes was confirmed by its colocalization with ER-Tracker Blue-White DPX dye (Fig. 4*C*). This colocalization is further supported by the overlapping of pixel intensities in the linescan plot (Fig. 4*C*, Linescan intensity plot, marked with black arrows), as well as the high positive Pearson correlation coefficient value (Fig. 4*C*, mentioned within the intensity plot). Similarly, the subcellular distribution of α-SNAP1 was determined in fixed wild-type promastigotes using rabbit anti-α-SNAP1 antibody and it's corresponding fluorescently-probed secondary antibody. Two bright punctate dots of α-SNAP1 were predominantly observed near the anterior part of the cell: one dot proximal to the FP [Fig. 4*D*, upper panel, marked with white arrows; and Fig. S4, *A* and *B* (cropped version of Fig. 4*D* upper panel), marked with white arrows], while the other was found in the endosomal compartment, positioned juxtaposed

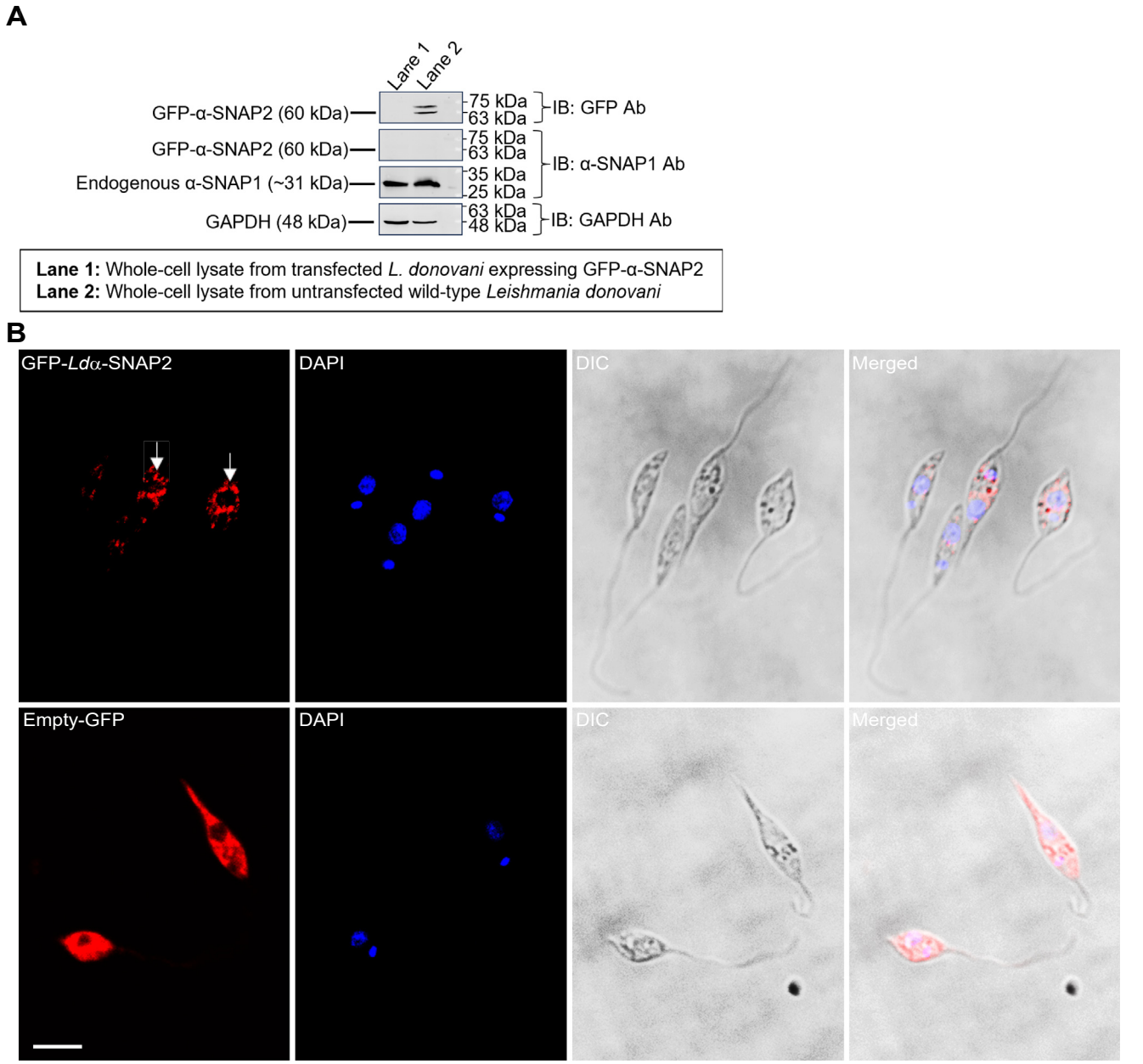

Figure 4. Antibody specificity of the anti-*Ld*α-SNAP1 antibody and subcellular distribution of *Ld*α-SNAP paralogs in *L. donovani* promastigotes. *A*, whole-cell lysates of wild-type untransfected promastigotes and the transfected promastigotes expressing GFP tagged α-SNAP2 were subjected to western immunoblotting and probed with anti-α-SNAP1 antibody to determine the antibody specificity. Anti-GFP antibody was used to detect the presence of GFP-fused α-SNAP2 in the lysate. GAPDH was used as a loading control. *B*, immunolocalization of GFP-fused α-SNAP2 (*upper panel*) and empty GFP (*lower panel*) in formaldehyde-fixed promastigotes using anti-GFP antibody. *White* arrows mark the ER. Each experiment was performed in triplicate, with three technical replicates for each. Scale bar: 4.6 μm. *C*, colocalization of GFP fused α-SNAP2 with the ER-Tracker Blue-White DPX dye in live promastigotes. Each experiment was performed in triplicate, with three technical replicates for each. Scale bar: 5 μm; The intensity profile graph of GFP fused *Ld*α-SNAP2 colocalization with the ER-Tracker dye. The pixel intensity in each channel is measured along the marked *white* line drawn on the image and has been plotted *versus* the distance along the line. The Line scan graph from single confocal planes shows the pixel intensity along the freely positioned line of ER-Tracker dye, and GFP fused *Ld*α-SNAP2. The *black* arrows indicate the position of pixel intensity overlapping. The calculated Pearson correlation coefficient value (r) for this pair of fluorescence signals is mentioned within the intensity plot. *D*, immunolocalization with the anti-α-SNAP1 antibody of endogenous α-SNAP1 at diverse intracellular compartments (*top panel*) of fixed and permeabilized promastigotes. Localizations at the FP, endosomal compartment, and membrane-bound sensors or flagellar attachment plaques are shown in *white*, *orange*, and *yellow arrows*, respectively. The *bottom panel* shows the formaldehyde-fixed promastigotes stained with pre-immune sera, representing the negative control. Each experiment was performed in triplicate, with three technical replicates for each. Scale bar: 10 μm. *E*, live cell immunolocalization of *Ld*α-SNAP1 in Golgi-specific Bodipy-TR ceramide-stained promastigotes. The *Ld*α-SNAP1 is shown in *green*, while the *red* represents the Golgi. Each experiment was performed in triplicate, with three technical replicates for each. Scale bar: 10 μm; The linescan intensity plot for detecting the colocalization between *Ld*α-SNAP1 and the Bodipy-TR ceramide dye at the *Leishmania* Golgi. The pixel intensity in each channel is measured along the marked *white* line drawn on the image and has been plotted *versus* the distance along the line. The Line scan graph from single confocal planes shows the fluorescence intensity along the freely positioned line of Bodipy-TR ceramide and *Ld*α-SNAP1. The calculated Pearson correlation coefficient value (r) for this pair of fluorescence signals is mentioned within the intensity plot. *F*(a) and (b) Colocalization study (with/without preincubation of promastigotes at 37 °C for 4 h) between *Ld*α-SNAP1 and GP63 in formaldehyde-fixed promastigotes, using anti-α-SNAP1 and anti-GP63 antibodies. The *Ld*α-SNAP1 at the FP and endosomal compartment are shown in *green*, and GP63 at the cell surface and FP in *red* (*top panels*). The *bottom panels* show formaldehyde-fixed promastigotes (with/without preincubation of promastigotes at 37 °C for 4 h before fixing) stained with pre-immune sera and GP63 antibody, representing the control (*bottom panels*). White arrows represent the colocalization of GP63 and α-SNAP1 at FP, and *white* arrowheads

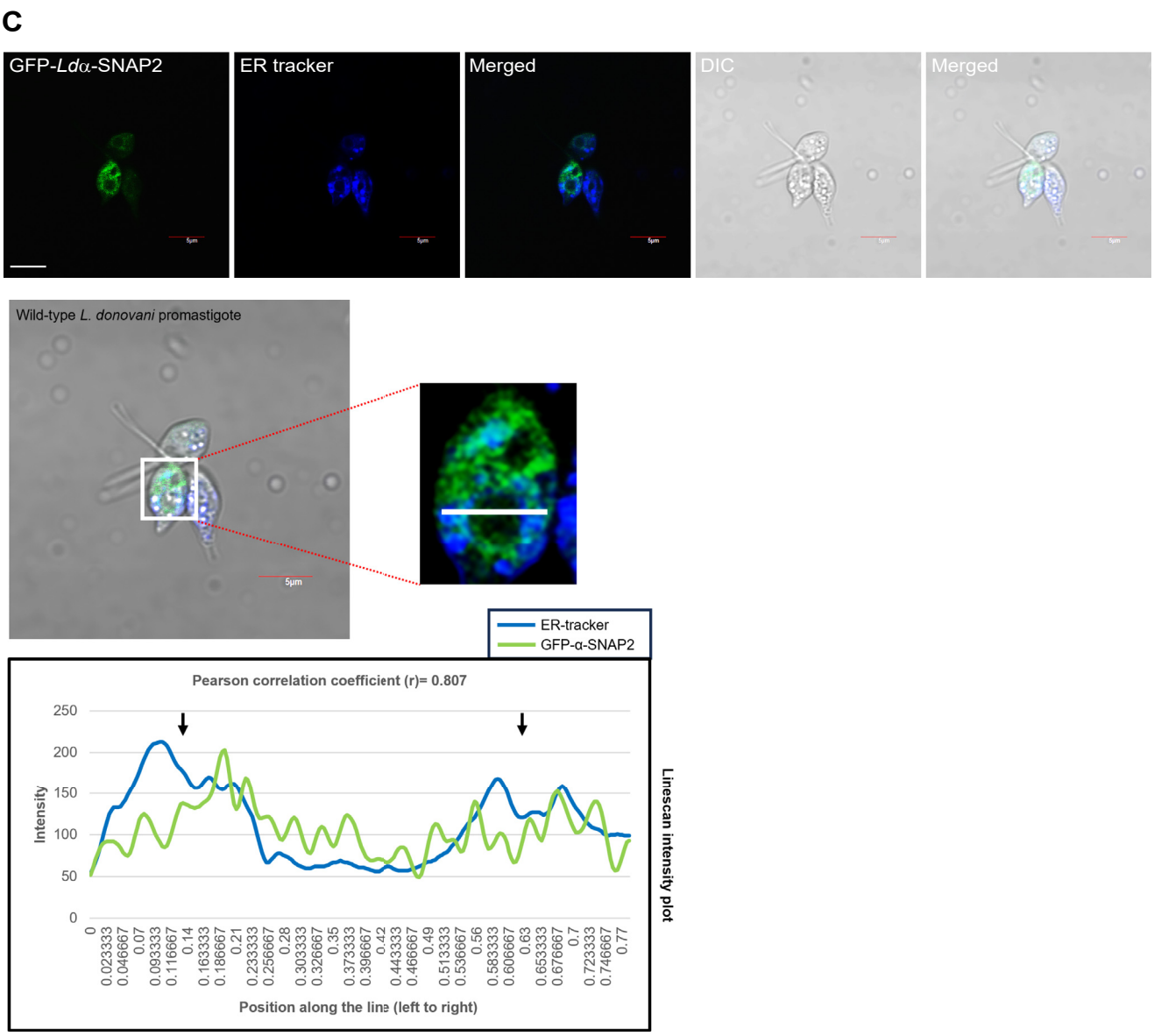

Figure 4. (*continued*).

to kinetoplast (Fig. 4*D*, upper panel, marked with orange arrows; Fig. S4, *A* and *B*, marked with orange arrows; and Fig. S4*C*, marked with white arrow) (51, 52). A negative control experiment using rabbit isotype-specific or pre-immune sera under the same conditions did not yield any signal in our immunolocalization study (Fig. 4*D*, lower panel). Besteiro *et al.* documented the intracellular distribution of the Qa group of *L. major* SNAREs in the Golgi, late endosome or lysosome, and the FP (14). Given that α-SNAP interacts with the SNARE monomers to disassemble the cis-SNARE complex, the localization of *Ld*α-SNAP1 near the FP and endosomal compartment suggests their possible collaborative function with the Qa SNAREs at these sites (51, 52). Apart from these usual locations, a small fraction of *Ld*α-SNAP1 was also found associated with the flagellum of some promastigotes, indicating its likely connection with the membrane-bound sensors and/or the flagellar attachment plaque [Fig. 4*D*, upper panel, marked with yellow arrows; and Fig. S4*B* (cropped version of Fig. 4*D* upper panel), marked with yellow arrows] (53–55).

The Golgi apparatus in *Leishmania* spp. is consistently located parallel to the FP, slightly tilted towards the flagellar side, near the beginning of the flagellum (56, 57). Since a

indicate FP in promastigotes. Each experiment was performed in triplicate, with three technical replicates for each. Scale bar: 5 μm; The linescan intensity graph for detecting the colocalization between *Ld*α-SNAP1 and the *Leishmania* surface protease GP63 at the FP region with/without preincubation of promastigotes at 37 °C for 4 h. The pixel intensity in each channel is measured along the marked white line drawn on the images and has been plotted *versus* the distance along the line. The Line scan graph from single confocal planes shows the fluorescence intensity along the freely positioned line of *Ld*α-SNAP1 and GP63. The *Black arrows* indicate the position of the pixel intensity overlapping. The Pearson correlation coefficient value (r) for each pair of fluorescence signals is mentioned within their respective intensity plot.

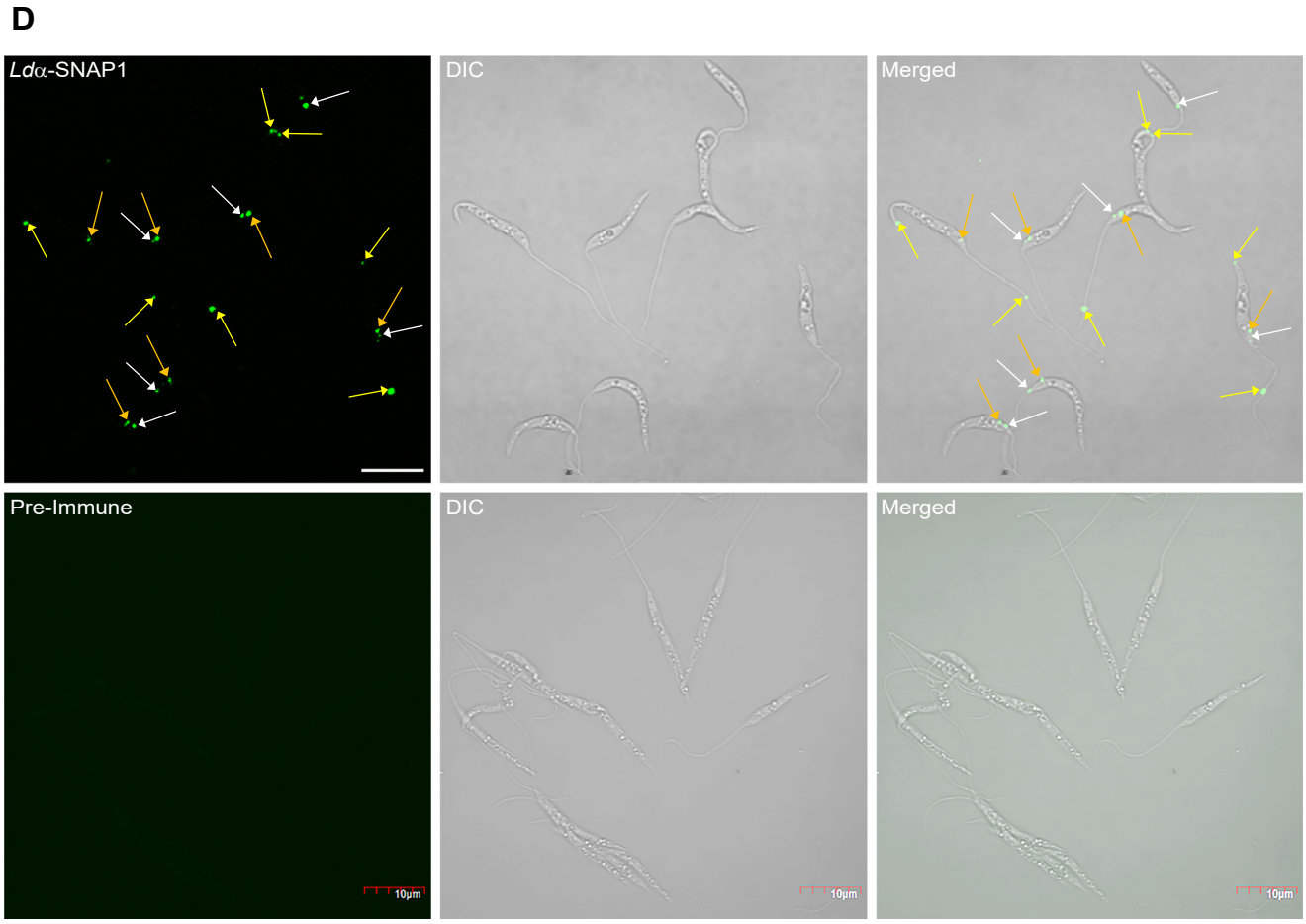

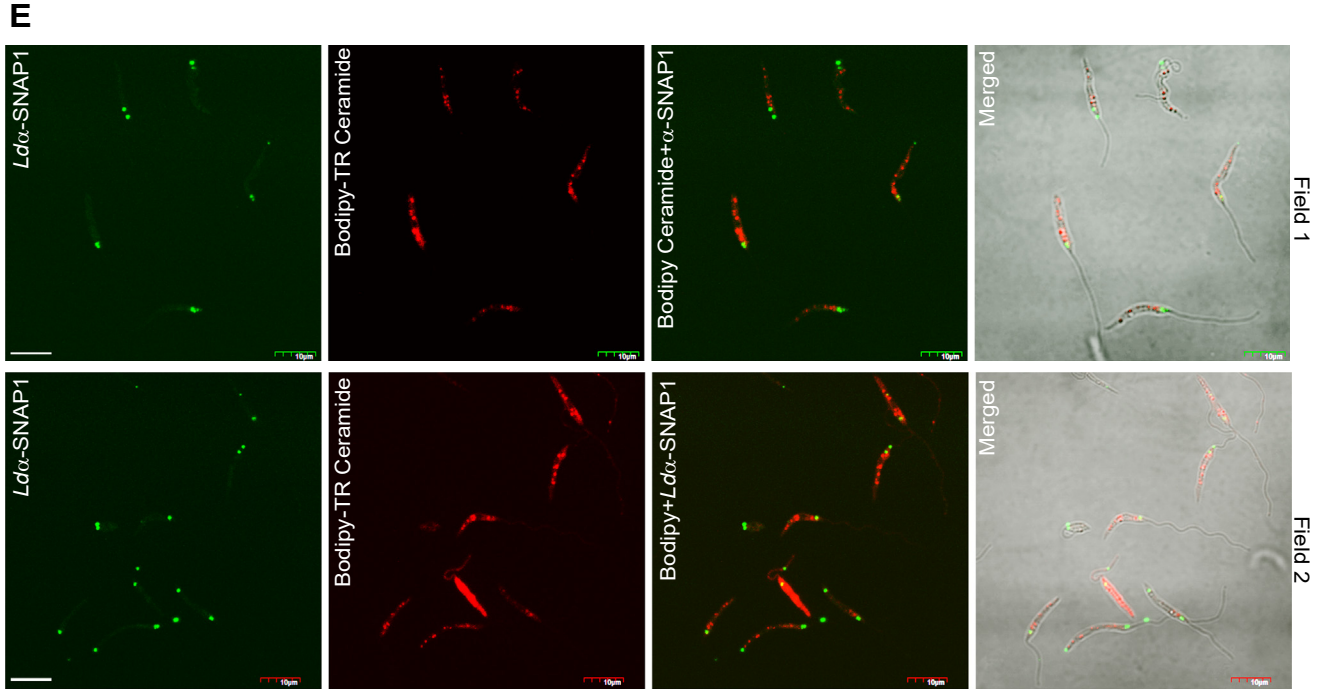

Figure 4. (*continued*).

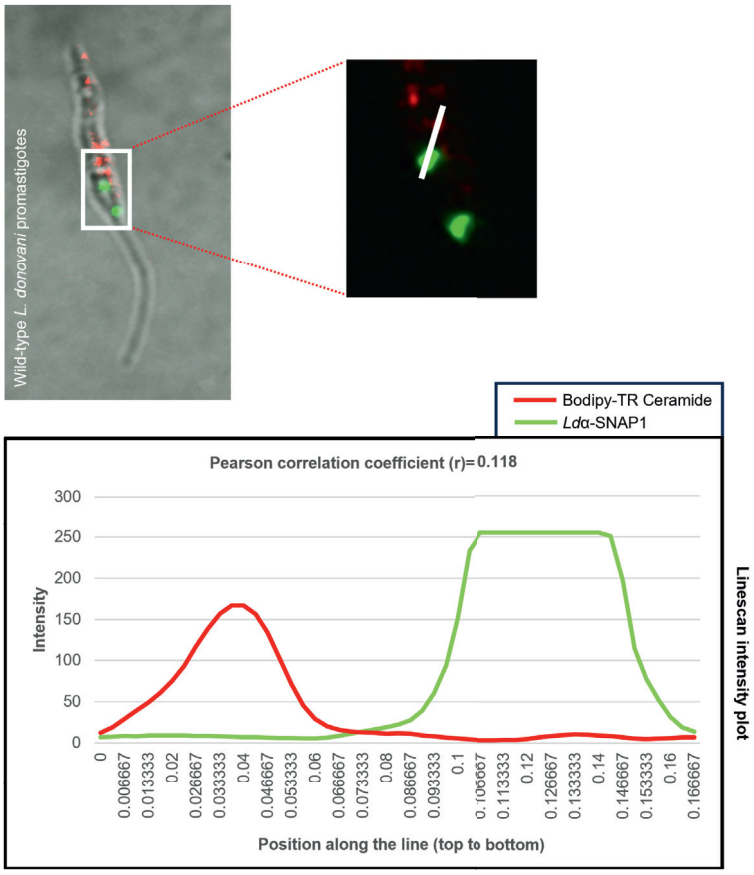

F(a)

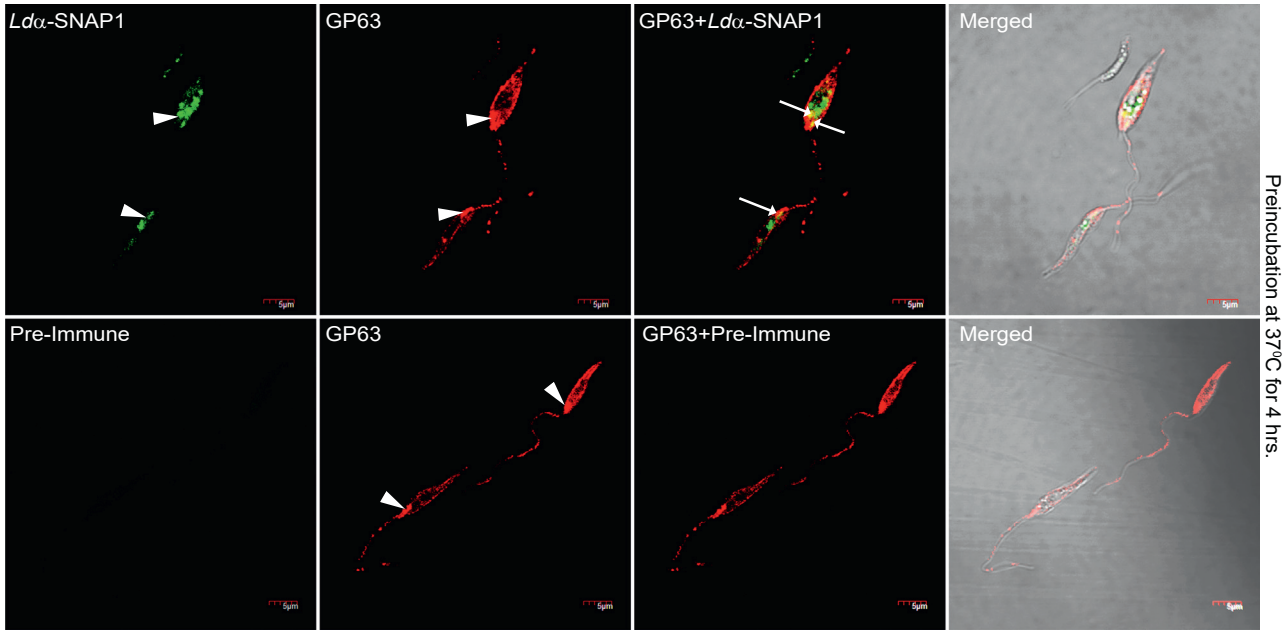

Figure 4. (*continued*).

previous study reported that Qa SNAREs are localized at the Golgi of *Leishmania*, and most of the *Ldα*-SNAP1 is also found near the FP, we attempted to determine whether the *Ldα*-SNAP1 localizes at the Golgi (14). We first stained promastigotes with a Golgi-specific fluorescent ceramide analog, Bodipy-TR ceramide (57). Following this, we

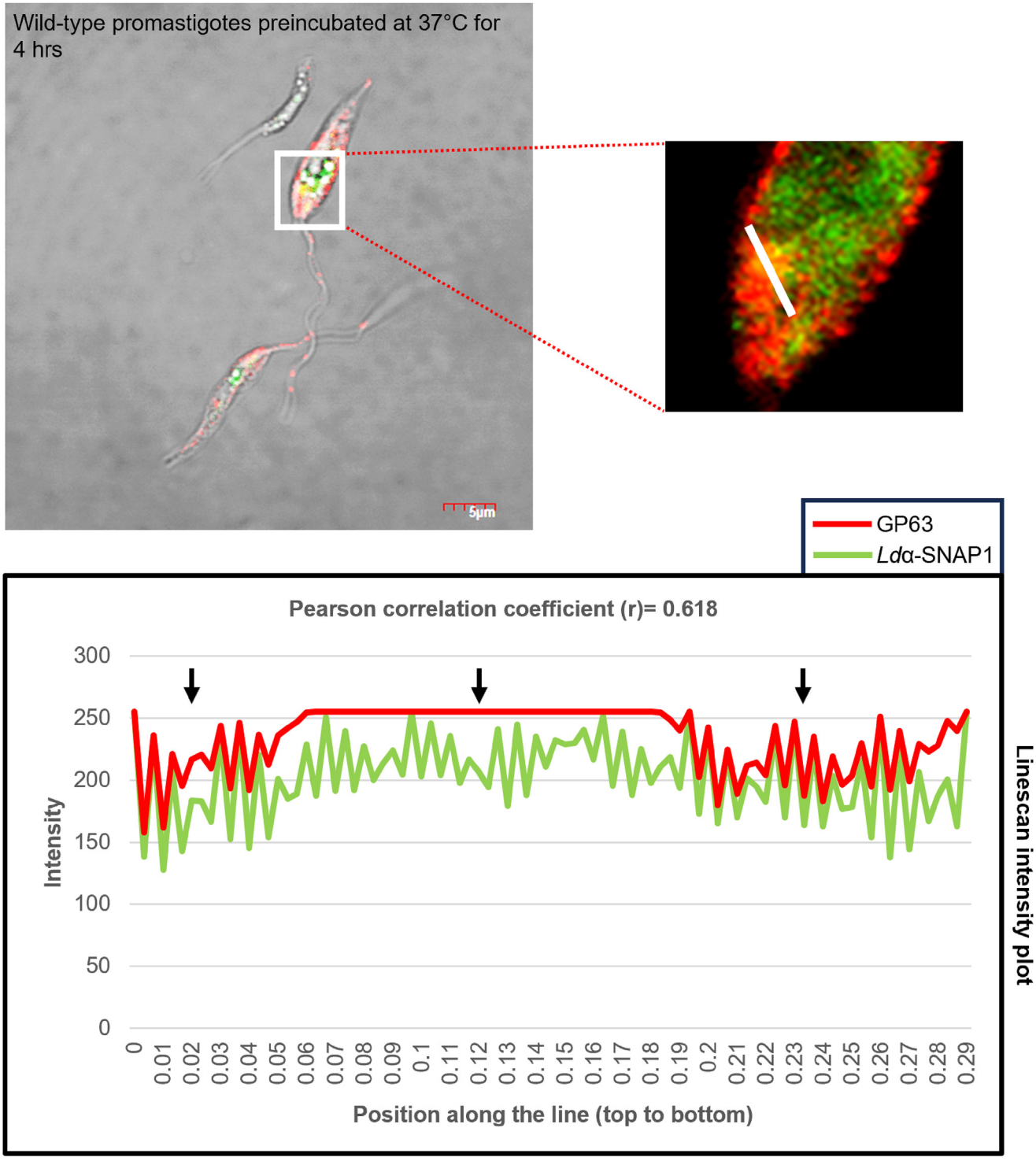

Figure 4. (*continued*).

performed live-cell immunolabeling using anti-α-SNAP1 antibody. However, our colocalization study revealed no overlap between the *Ld*α-SNAP1 (green) and the Golgi marker (red) signals, as the green and red dots appeared independently without any superimposition [Fig. 4*E*, Field 1 and 2; and Fig. S5 (cropped version of Fig. 4*E* Field 1), marked with black arrows and an arrowhead). This observation is supported by our linescan intensity plot, where the peaks of red and green pixel intensities were visualized individually without any overlapping between them (Fig. 4*E*, Linescan intensity plot), as well as low Pearson correlation coefficient value (Fig. 4*E*, mentioned within the Linescan intensity plot).

Previous studies have shown that the leishmanial metalloprotease GP63 is synthesized in the ER and secreted into the extracellular milieu from FP and cell surface (4, 5). Consequently, we sought to investigate if there is any crosstalk

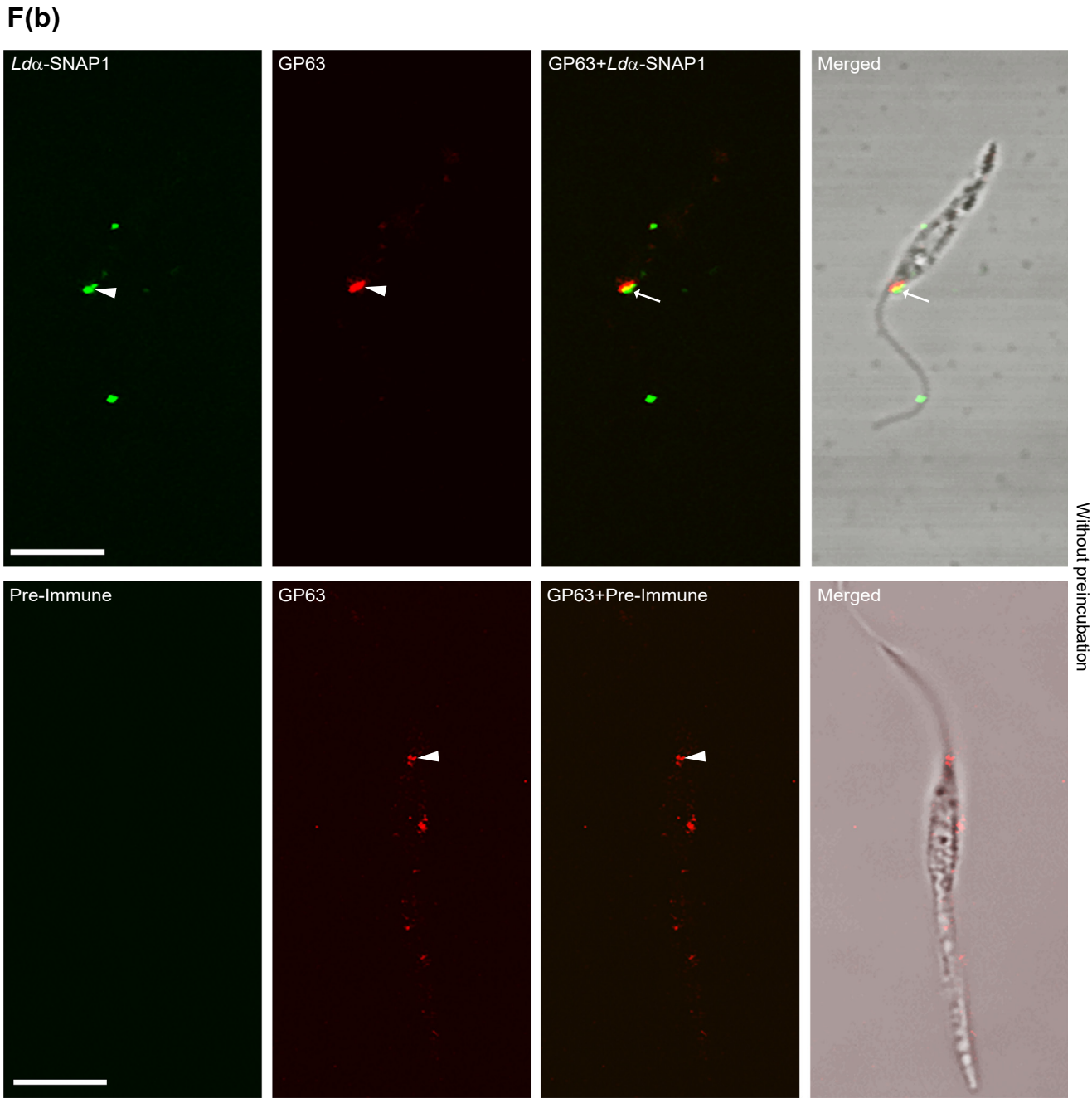

Figure 4. (*continued*).

between the *Ldα*-SNAP1 and GP63 at the FP of promastigotes. Literature indicates that a temperature shift from ambient (*i.e.*, 25 °C) to 37 °C induces a sudden rise in protein secretion from *Leishmania* spp., within 4 h, mimicking the parasite's entry into vertebrate host (58, 59). Through an *in vivo* colocalization analysis between *Ldα*-SNAP1 and GP63 in promastigotes, with/without preincubation at 37 °C for 4 h before fixing and immunofluorescence (IF). We employed anti-α-SNAP1 and anti-GP63 antibodies along with their corresponding fluorophore-coupled secondary antibodies. Our observation revealed a significant spatial overlap between GP63 and *Ldα*-SNAP1 signals at the FP under both conditions [Fig. 4, *F*(a) and *F*(b), Upper panels, marked with white arrows; Fig. S6, A and *B*, Field one and 2, marked with white arrowheads]. This overlap is confirmed by linescan intensity plot (Fig. 4, *F*(a) and *F*(b), Linescan intensity plot, marked with black arrows) as well as high positive Pearson correlation coefficient value (Fig. 4, *F*(a) and *F*(b), mentioned within the linescan intensity plots). Negative control, using pre-immune rabbit serum showed no detectable signal in the IF study [Fig. 4, *F*(a) and *F*(b), lower panels]. Hence, the localization of *Ldα*-SNAP1 at the FP and endosomal compartment, where Qa SNAREs LmjF28.1470

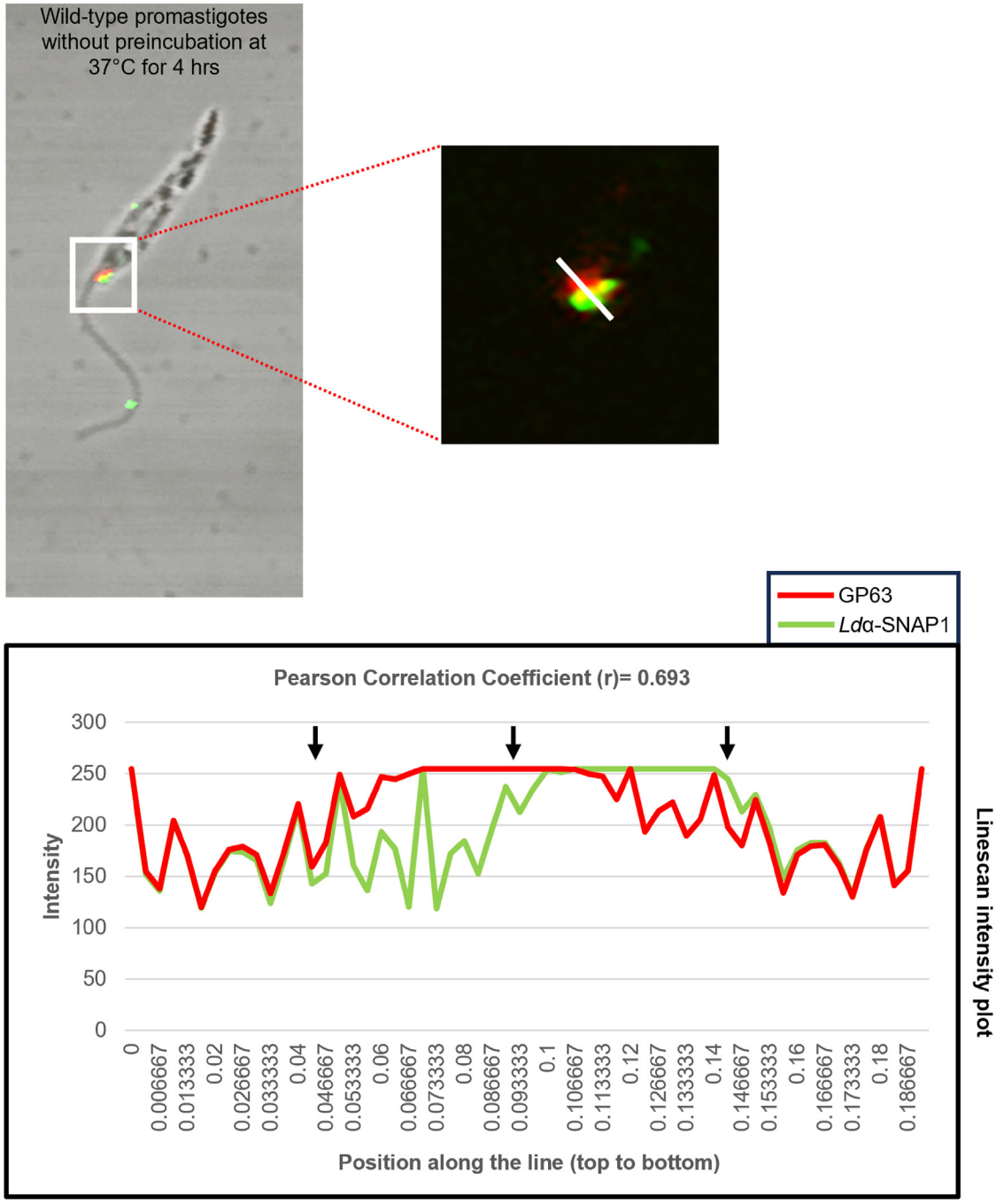

Figure 4. (*continued*).

and LmjF19.0120, respectively, are known to reside (14), hints its role in cis-SNARE bundle disassembly at these sites. Since both *Ld*α-SNAP1 and Qa SNAREs LmjF28.1470 share common intracellular distribution at the FP, we hypothesize that these proteins are likely involved in the disassembly of cis-SNARE complex at the FP. Additionally, our IF study showed colocalization between *Ld*α-SNAP1 and GP63 in the FP, indicating that the SNARE bundle disassembly might promote the fusion of GP63-containing vesicles with the FP membrane, a prerequisite event before exocytosis of GP63 into the extracellular space (5, 60).

The interaction and overlapping distribution of Ld*NSF and* Ldα*-SNAP1 at the FP strongly suggest their involvement in disassembling cis-SNARE complexes in this region*

The role of α-SNAP in unwinding the cis-SNARE bundle during vesicular trafficking depends on its coupling with the ATPase NSF, where it serves as an adaptor for NSF. Both *Ld*α-SNAP1 and leishmanial Qa SNARE *LmjF*28.1470 have been detected in the FP of promastigotes. The presence of *Ld*NSF in this region would confirm the participation of *Ld*α-SNAP1 in cis-SNARE complex unzippering and promoting the fusion of GP63-containing vesicles with the FP

membrane. To further investigate, we determine *Ld*NSF's intracellular localization in Bodipy-TR ceramide-stained promastigotes using live cell IF with rabbit anti-NSF antibody. We observed a distinct punctate distribution of *Ld*NSF near the FP. This localization was similar to Qa SNARE LmjF28.1470 and *Ld*α-SNAP1 (Fig. 5*A*). Importantly, *Ld*NSF (green) did not significantly overlap with the fluorescent signals of Golgi marker Bodipy-TR ceramide (red) in our colocalization study [Figs. 5*A*; and S7 (cropped version of Fig. 5*A*), Field one and 2, marked with the black arrow and arrow head]. This finding is further confirmed by the linescan intensity plot (Fig. 5*A*, Linescan intensity plot), where the peaks of red and green pixel intensities were visualized independently without any overlapping between them, as well as low Pearson correlation coefficient value (Fig. 5*A*, mentioned within the Linescan intensity plot). The results suggest that *Ld*NSF is explicitly localized at the FP, identical to its adaptor *Ld*α-SNAP1. The involvement of *Ld*α-SNAP1 and *Ld*NSF in SNARE unpairing can be confirmed through their physical association. Due to the use of rabbit-raised antibodies for both proteins, colocalization analysis *via* IF staining is not feasible because of cross-reactivity. Instead, we used an immunoprecipitation (IP) approach with protein lysate from the promastigotes. The leishmanial whole-cell

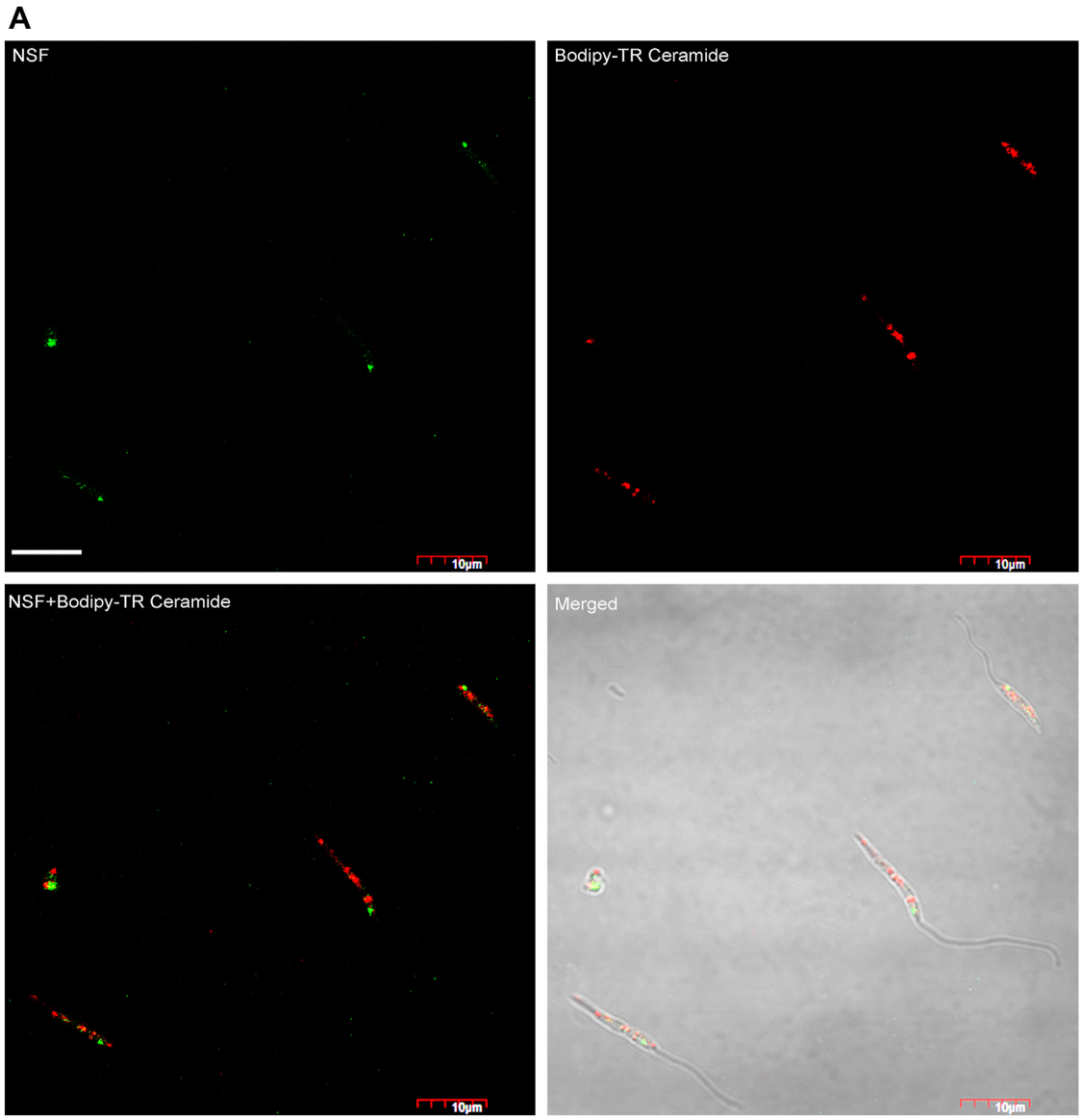

Figure 5. Immunolocalization of *Ld*NSF and its association with *Ld*α-SNAP1. *A*, immunolocalization of *Ld*NSF in Bodipy-TR ceramide-stained mid-log phase live promastigotes. The *Ld*NSF at FP is shown in *green*, while the *red* represents the Golgi. Each experiment was performed in triplicate, with three technical replicates for each. Scale bar: 10 µm; An intensity profile graph of *Ld*NSF colocalization with the Bodipy-TR ceramide dye at the leishmanial Golgi. The pixel intensity in each channel is measured along the marked *white* line drawn on the image and has been plotted *versus* the distance along the line. The Line scan graph from single confocal planes shows the pixel intensity along the freely positioned line of Bodipy-TR ceramide and *Ld*NSF. The calculated Pearson correlation coefficient value (r) for this pair of fluorescence signals is mentioned within the intensity plot. *B*, whole-cell lysates of promastigotes were subjected to immunoprecipitation with (test) or without (negative control) anti-*Ld*α-SNAP1 antibody followed by western immunoblotting (Lane 1 and 2). Whereas lanes 3 and 4 represent WB with the whole-cell lysates (used for the IP experiment) to detect the presence of NSF and α-SNAP1 in the given lysates. Both the blots were probed with anti-α-SNAP1 and anti-NSF antibodies. M stands for protein size marker.

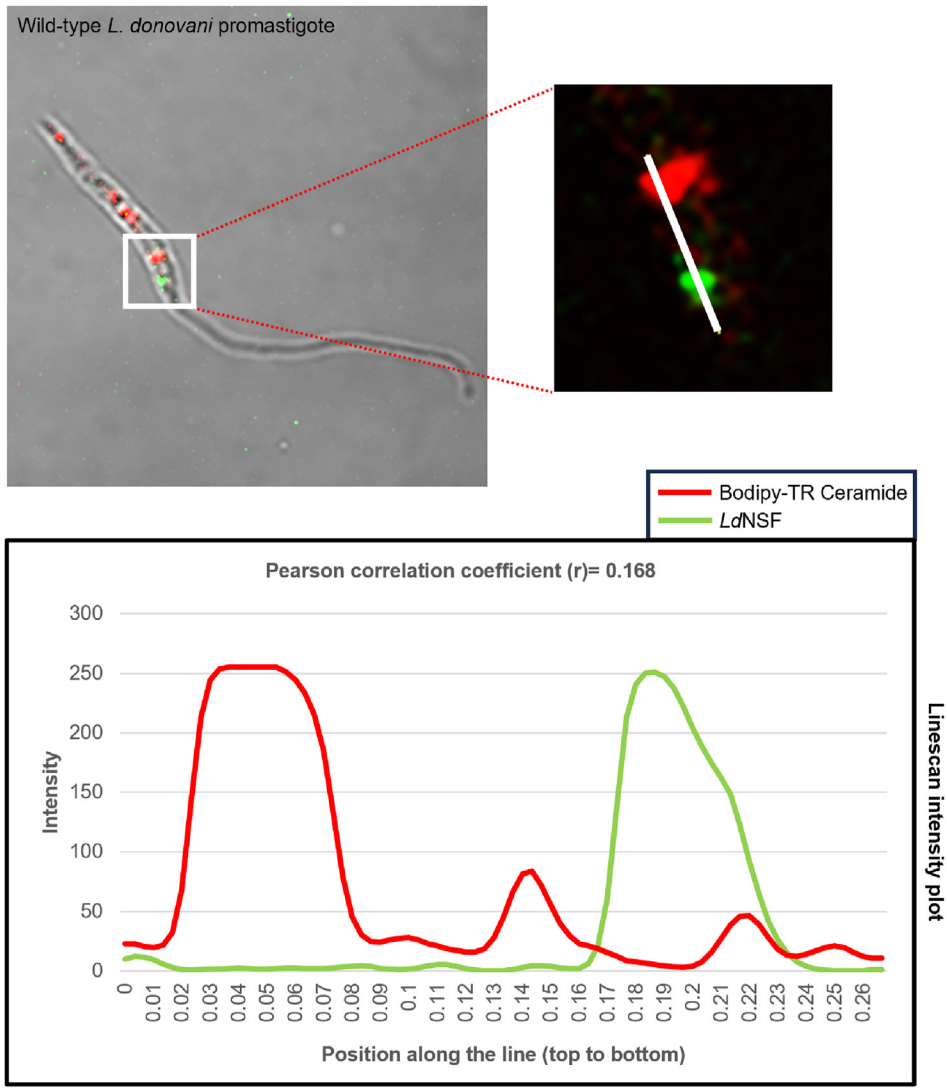

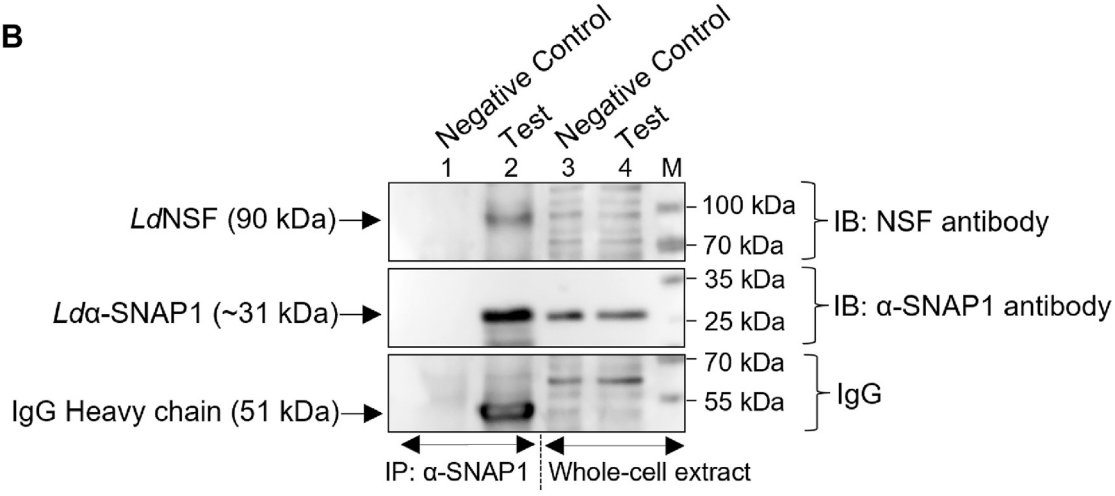

Figure 5. (*continued*).

lysate was immunoprecipitated using an anti-α-SNAP1 antibody, followed by WB with both *Ld*NSF and *Ld*α-SNAP1 antibodies, revealing a strong interaction between the two (Fig. 5*B*, Lane 2). No bands corresponding to *Ld*NSF and *Ld*α-SNAP1 were detected in the negative control (Lane 1). Further WB analysis confirmed the presence of both proteins

in the test and negative control lysates, with the antibodies successfully recognizing their respective targets (Fig. 5*B*, Lanes 3 and 4). These findings provide significant insight into the coordinated roles of *Ld*α-SNAP1, *Ld*NSF, and Qa SNARE LmjF28.1470 in vesicle fusion at the FP. Furthermore, our present observations, along with previous studies: a) *Ld*α-SNAP1, *Ld*NSF, and Qa SNARE LmjF28.1470 localize at the FP of *Leishmania*, b) an interaction between *Ld*α-SNAP1 and *Ld*NSF in Co-IP experiment, c) colocalization between *Ld*α-SNAP1 and GP63 at the FP of *Leishmania*, d) Qa SNARE LmjF28.1470 plays a role in the exchange of cellular materials with extracellular milieu, e) the fusion of vesicles (containing the membrane-bound and free GP63) with FP membrane before the exocytosis of GP63, and f) vesicular trafficking-mediated secretion of unmodified-GP63 into the extracellular milieu through the FP, collectively indicate a role of *Ld*α-SNAP1 (in association with *Ld*NSF and *Ld*SNAREs) in facilitating the fusion of GP63-containing vesicles with the FP membrane of *L. donovani* promastigotes (5, 14, 60). This is further supported by a previous observation, where α-SNAP is concentrated at the nerve terminals of crayfish neurons to form and maintain a readily releasable pool of synaptic vesicles, promoting neurotransmitter release (61). Therefore, we assume that *Ld*α-SNAP1 may also promote exocytosis of GP63 from the FP, as it serves as the primary site for the release of virulence factors by promastigotes. Incidentally, some of the GP63 molecules have been reported to be released directly *via* vesicular trafficking through the FP of *Leishmania*, which further supports our assumption (5, 62–64).

The C-terminal leucine, essential for stimulating NSF's ATPase activity during vesicular trafficking, is conserved in both Ldα*-SNAPs, confirming their involvement in GP63 transport and possibly its exocytosis*

During vesicular transport, NSF, in combination with its adaptor α-SNAP, facilitates ATP hydrolysis-dependent disassembly of the pre-formed cis-SNARE complex on the acceptor membrane. It triggers vesicle fusion to the target membrane (7–9). α-SNAP can stimulate NSF's activity by binding to its N-terminal as well as C-terminal fragments and helping with ATP hydrolysis. A conserved leucine towards the C-terminal end of α-SNAP is crucial for stimulating the NSF's ATPase activity and efficient cis-SNARE bundle unzippering (16). Mutation of this conserved leucine or truncation of the C-terminal 10 amino acids in α-SNAP significantly reduces ATPase activity of NSF (16). We found that only *Ld*α-SNAP1 shows localization similar to *Ld*NSF and can interact with it, though *Ld*α-SNAP2 may also participate in SNARE unpairing (because of the presence of conserved SNARE-interacting residues at the concave face) through coupling with NSF at a distinct location. To test whether the key leucine residue is conserved in both *Ld*α-SNAP paralogs, we carried out MSA. Our MSA of C-terminal ten amino acids of α-SNAP orthologs from diverse eukaryotes, including two paralogs from *Leishmania*, showed that the leucine is conserved in both *Ld*α-SNAPs (Leucine-281 in *Ld*α-SNAP1 and Leucine-290 in *Ld*α-SNAP2) (Fig. 6*A*, marked with a black box and asterisk). This suggests that both paralogs can stimulate the ATPase activity of NSF. We have previously demonstrated the differential localization of *Ld*α-SNAP2 and *Ld*α-SNAP1 in the ER (where the GP63 proteases are synthesized) and FP (from where exocytosis of GP63 occurs), respectively, along with the colocalization between *Ld*α-SNAP1 and GP63 at the FP. Given the conservation of C-terminal leucine in both *Ld*α-SNAPs, we next tried to find out whether both paralogs are involved in the secretory transport of GP63 from its site of synthesis. We transfected the constructs pXG-GFP^{+2}-*Ld*α-SNAP1$_{(L281A)}$ and pXG-GFP^{+2}-*Ld*α-SNAP2$_{(L290A)}$ separately to express GFP-fused *Ld*α-SNAP1$_{(L281A)}$ and *Ld*α-SNAP2$_{(L290A)}$ mutant proteins within promastigotes. We then used IF and confocal microscopy on formaldehyde-fixed promastigotes, pre-incubated at 37 °C for 4 h, to determine the localization of GP63 and its colocalization with the mutant *Ld*α-SNAPs. Primary antibodies against the GFP-tag and GP63, along with fluorochrome-labeled secondary antibodies, were employed for detection. The results of the IF study displayed a diffuse cytosolic fluorescence corresponding to GFP-fused *Ld*α-SNAP1$_{(L281A)}$ proteins (Figs. 6*B*, upper panel and S8, upper panels of Field 1 and 2), indicating its mislocalization due to single point mutation in the conserved C-terminal leucine residue [Compare Fig. 6*B*, top panel with Fig. 4*D*, top panel; Compare Fig. 6*C*(b) with Fig. 6*C*(a)]. This finding is further supported by the cytosolic distribution of GP63, suggesting that the fusion of GP63-containing vesicles with the FP membrane and the subsequent exocytosis of GP63 from FP and cell surface are likely affected following overexpression of mutant *Ld*α-SNAP1$_{(L281A)}$ [Fig. 6*B*, top panel; compare with Fig. 4, *F*(a) and *F*(b), top panels; and also compare with Fig. S6, *A* and *B*, Field 1 and 2]. This assumption is supported by an existing report, where overexpression of dominant negative α-SNAP(L294A) has been shown to inhibit the neurotransmitter release at the synapse (61). Similarly, the cytosolic distribution of GP63 was also observed following overexpression of GFP-fused *Ld*α-SNAP2$_{(L290A)}$ [Fig. 6*B*, bottom panel; compare with Fig. 4, *F*(a) and *F*(b), top panels; Compare Figs. 6, *C*(c) and *C*(a), and S6, *A* and *B*, Field 1 and 2, compare with Fig. 6*B*, bottom panel]. The mutant GFP-tagged *Ld*α-SNAP2$_{(L290A)}$ proteins showed a punctuated cytosolic distribution in formaldehyde-fixed promastigotes, similar to *Ld*α-SNAP1$_{(L281A)}$ (Fig. 6*B*, bottom panel and Fig. S8, bottom panels of Field one and 2) (Compare Fig. 6*B*, bottom panel with Fig. 4*B*, top panel). Existing literature shows overexpression of dominant negative *Ld*Sar1 mutant (LdSar1:T34N) blocks secretion of GP63 in *Leishmania* by disrupting its ER to Golgi transport (65). Since overexpression of GFP-*Ld*α-SNAP2$_{(L290A)}$ also causes mislocalization of GP63 (cytosolic distribution instead of localization at the FP and cell surface) [Compare Fig. 6*C*(c) with Fig. 6*C*(a)], we speculate that *Ld*α-SNAP2 might be involved in the trafficking of GP63-containing vesicles from ER to FP and the cell surface. However, this needs further exploration. Incidentally, some GP63 molecules may still be present at the cell periphery and FP of the transfected

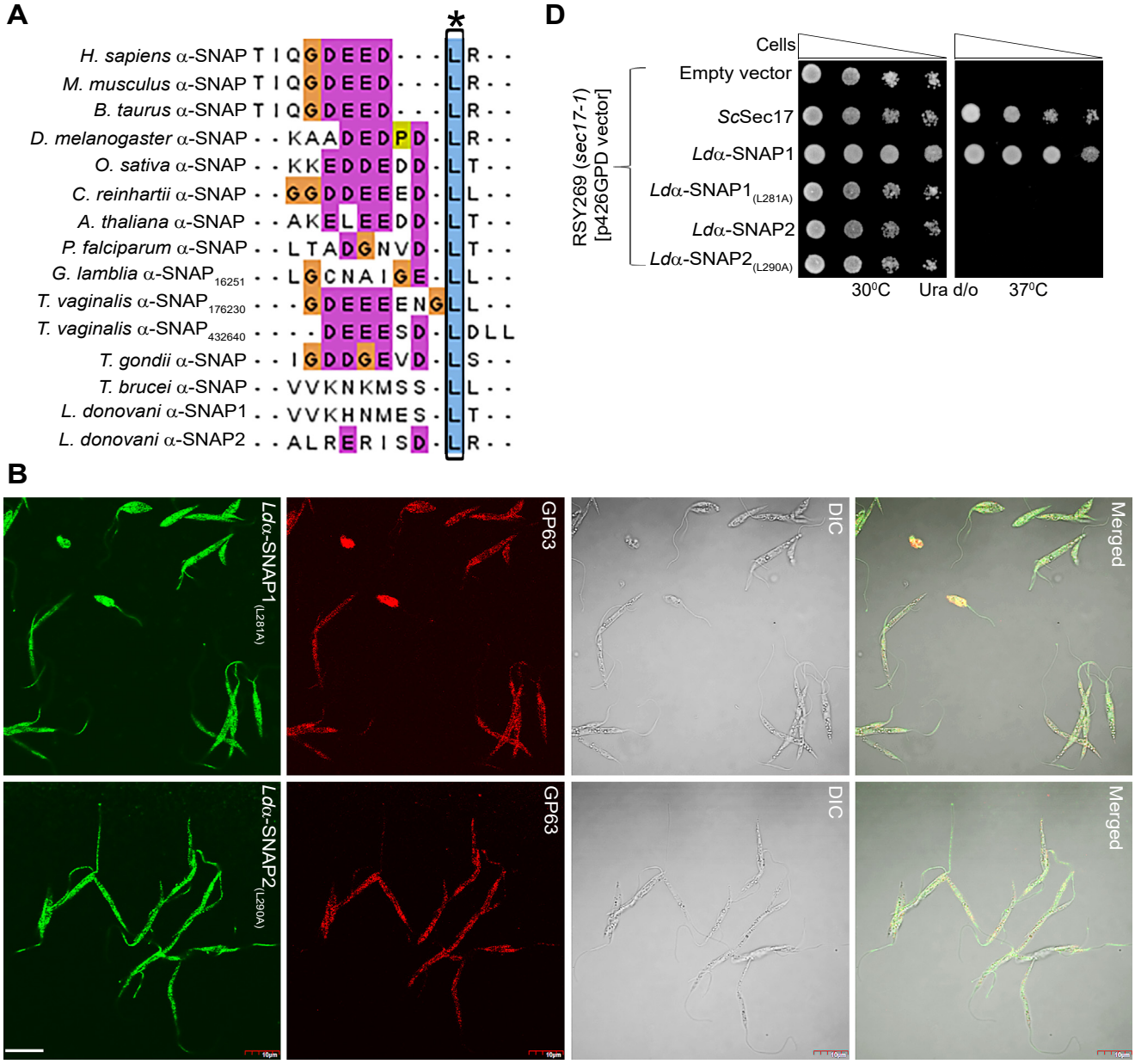

Figure 6. The essential role of C-terminally located conserved leucine of *Ldα*-SNAPs in the NSF-dependent trafficking function. *A*, multiple sequence alignment of the C-terminal 10 amino acids of α-SNAP orthologs from diverse taxonomic groups. The conserved leucine residue, which was reported to stimulate the ATPase activity of NSF during cis-SNARE complex disassembly, is marked in the sequence alignment file with a *black box* and *asterisk*. *B*, colocalization of GFP-fused *Ldα*-SNAP1$_{(L281A)}$ (*upper panel*) and *Ldα*-SNAP2$_{(L290A)}$ (*bottom panel*) with the metalloprotease GP63 in formaldehyde-fixed promastigotes (after preincubation at 37 °C for 4 h) through IF using anti-GFP and anti-GP63 antibodies. The localization of GFP-tagged α-SNAP1$_{(L281A)}$ and GFP-tagged α-SNAP2$_{(L290A)}$ proteins are shown in *green*, whereas GP63 is in *red*. Each experiment was performed in triplicate, with three technical replicates for each. Scale bar: 5 μm; *C*, comparison of intracellular distribution of GP63 between wild-type *L. donovani* promastigotes [(a)] and wild-type cells overexpressing either GFP-fused *Ldα*-SNAP1$_{(L281A)}$ [(b)] or GFP-fused *Ldα*-SNAP2$_{(L290A)}$ [(c)] after formaldehyde fixing (following preincubation of cells at 37 °C for 4 h) through IF using different microscopic fields. Insets show the localization of GP63 at the cell surface (in wild-type) or throughout the cytosol (in GFP-tagged *Ldα*-SNAP1$_{(L281A)}$ or *Ldα*-SNAP2$_{(L290A)}$ overexpressing wild-type). The *white* and *yellow* arrows indicate the presence of GP63 proteins in PM blebs and cytosol, respectively, whereas the distribution at the FP has been indicated using the *white* arrowheads. Each experiment was performed in triplicate, with three technical replicates for each. Scale bar: 5 μm; *D*, the yeast expression vector containing the wild-type *Ldα*-SNAP1, mutant *Ldα*-SNAP1$_{(L281A)}$, wild-type *Ldα*-SNAP2, and mutant *Ldα*-SNAP2$_{(L290A)}$ were individually transformed in yeast *sec17-1* hypomorph. Growth of these transformants at both permissive (30 °C) and nonpermissive temperature (37 °C) was assessed by spotting serial dilutions on yeast synthetic medium lacking uracil (Ura d/o). The yeast transformants carrying *SEC17* and empty vector were used as a positive and negative control, respectively.

promastigotes expressing the GFP-fused *Ldα*-SNAP1$_{(L281A)}$ and *Ldα*-SNAP2$_{(L290A)}$. This could be due to the presence of endogenously-expressed chromosomal copies of wild-type *Ldα*-SNAP1 and *Ldα*-SNAP2 proteins. Despite the transgenic overexpression of the α-SNAP mutants, we assume that the existing endogenous wild-type proteins, in association with *Ld*NSF and *Ld*SNAREs, may facilitate the transport (from ER) as well as fusion of GP63-containing vesicle to FP and cell surface to a certain extent. The functional complementation approach provided further evidence for the non-functionality

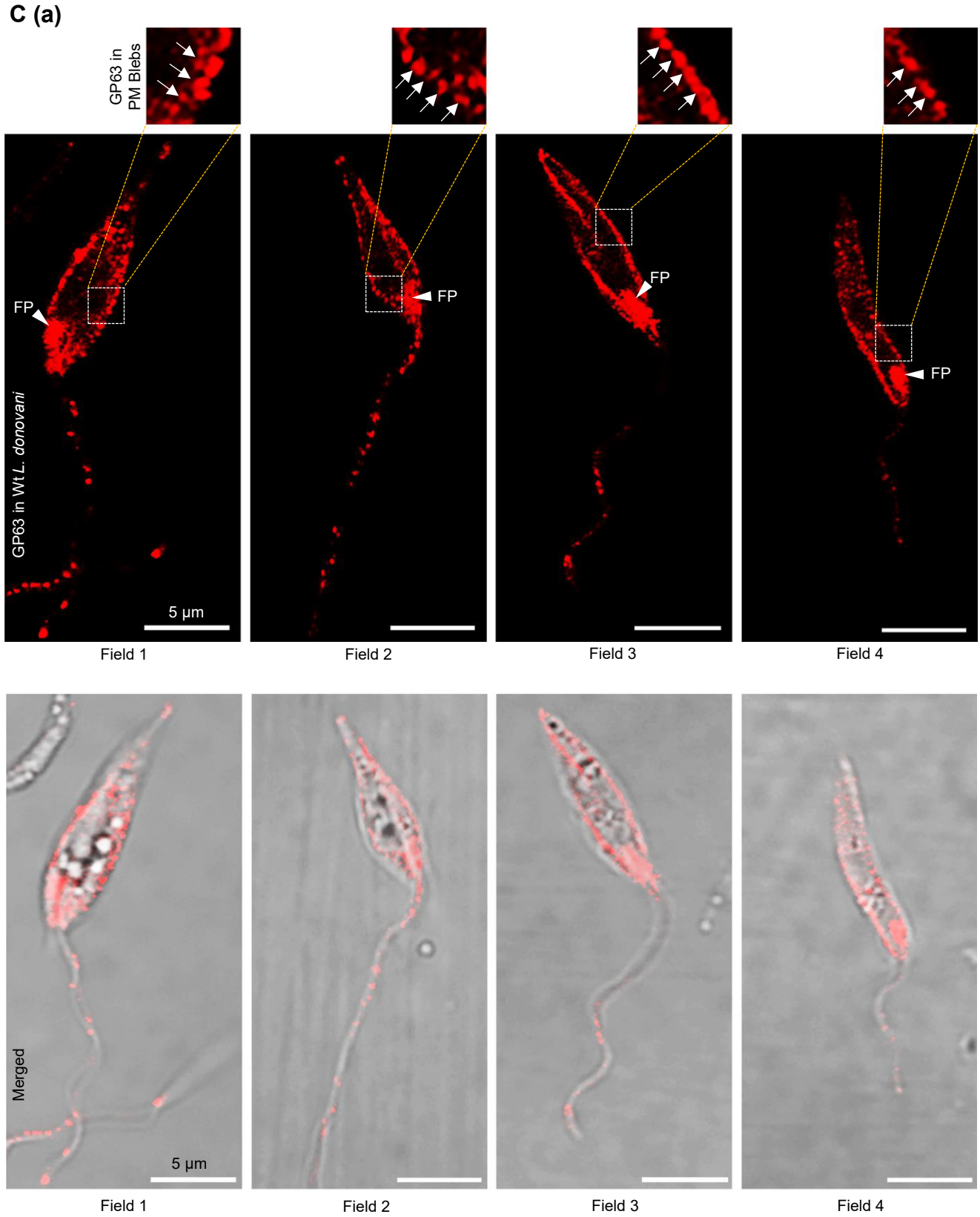

Figure 6. (*continued*).

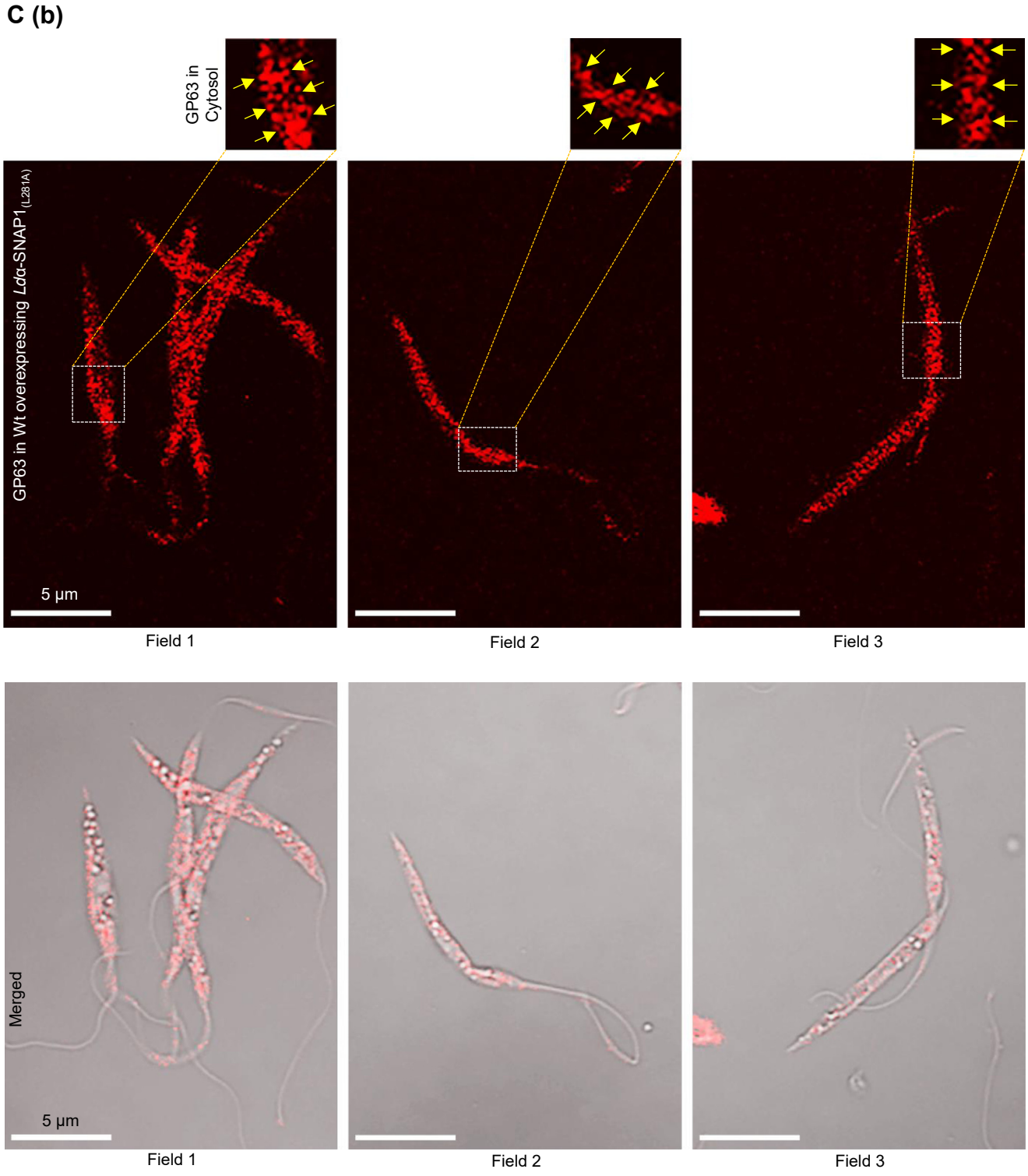

Figure 6. (*continued*).

of C-terminal leucine mutated *Ld*α-SNAPs. Constructs containing the mutated *Ld*α-SNAPs, p426GPD-*Ld*α-SNAP1$_{(L281A)}$ and p426GPD-*Ld*α-SNAP1$_{(L281A)}$, were transformed into yeast *sec17-1* hypomorphs, with wild-type *Ld*α-SNAP and *Sc*Sec17 as positive controls. The results showed that the transformants harboring the mutant *Ld*α-SNAPs failed to grow at 37 °C (Fig. 6*D*). The null phenotype in yeast hypomorph expressing *Ld*α-SNAP mutants at 37 °C indicates the non-functionality of mutant leishmanial proteins. Overall, these findings suggest that, like other eukaryotic α-SNAPs, the C-terminal leucine residue of *Ld*α-SNAPs is essential for stimulating NSF's ATPase activity during vesicle-mediated transport of cargo

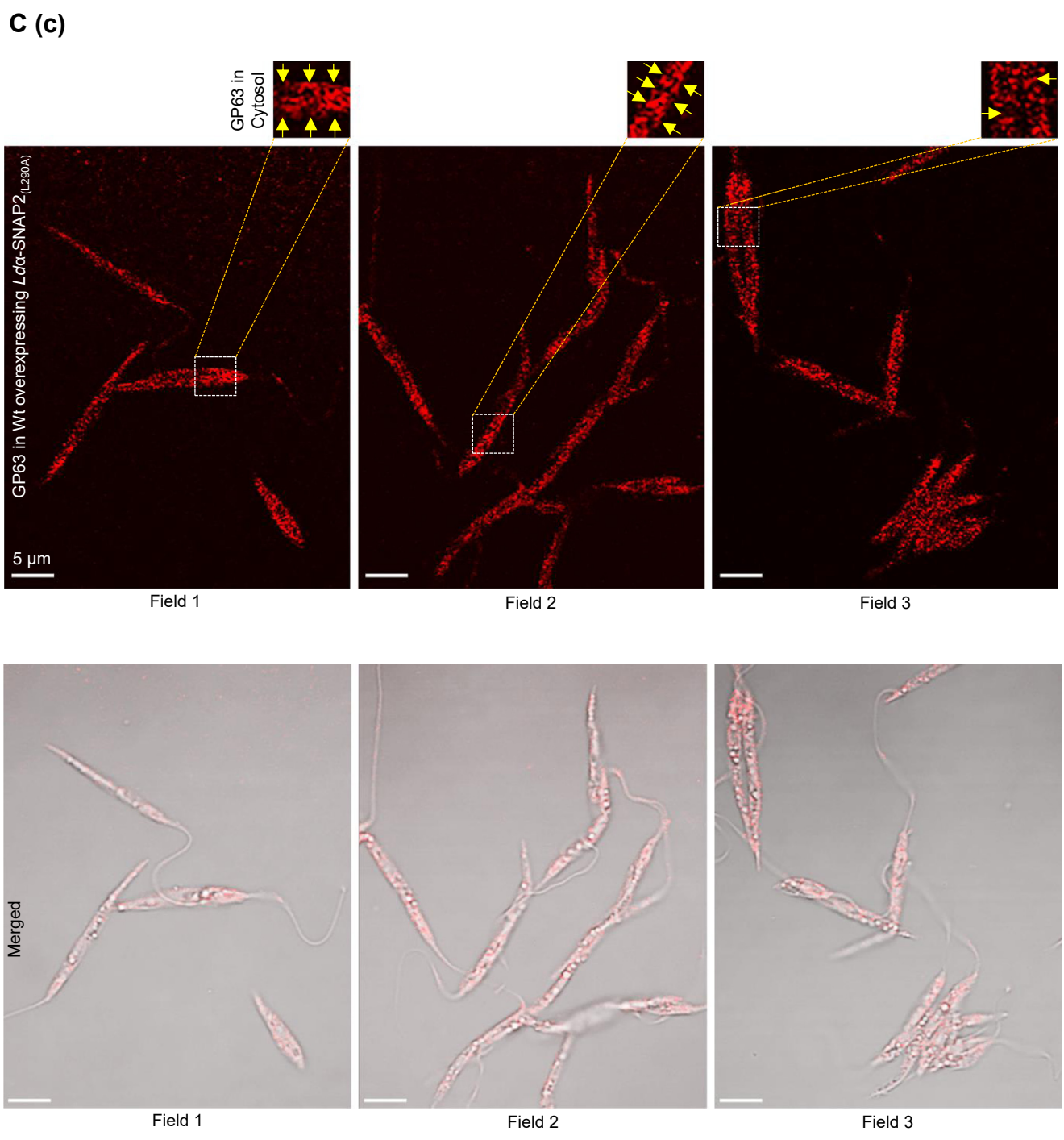

Figure 6. (*continued*).

molecules/virulence factors like GP63. Moreover, the impaired transport of GP63 from its site of synthesis (the ER) to its site of release (the FP and cell surface), along with inhibition of the fusion of GP63-containing vesicles with FP membrane following overexpression of mutant *Ld*α-SNAPs, indicate a subfunctionalization of both the *Ld*α-SNAP paralogs. This subfunctionalization occurs at distinct sites (the ER and FP) within promastigotes, facilitating the extracellular secretion of GP63, necessary for modulating the host's macrophage functions.

Discussion

Gene number expansion for adaptor protein α-SNAP in flagellated parasites is atypical among eukaryotes

Vesicular trafficking is crucial for transporting cellular materials and is conserved across Eukarya (66). However, parasites exhibit significant diversification in their membrane trafficking pathways due to the evolution of specific regulatory components. *Leishmania* exemplifies this, possessing two paralogs of the vesicle fusion component α-SNAP, while most

other eukaryotes have only one (14, 30). Other flagellated parasites also possess multiple copies of α-SNAP, whereas aflagellates typically have a single ortholog. This raises an important question about whether this duplication contributes to the survival of these parasitic and what the evolutionary and functional implications are of the unconventional expansion of α-SNAP orthologs within *Leishmania* spp (12, 13, 23, 30).

Nearly all structural features of canonical α-SNAP are conserved in the leishmanial α-SNAP paralogs

Multiple paralogs arise from intrachromosomal duplication of an ancestral gene, diverging over time (30, 67). Whole genome alignment study has shown that 4 to 16% of such chromosomal sequences may be falsely duplicated, impacting the copy number of many genes (68). The presence of two *Ld*α-SNAPs on chromosomes 20 and 32 suggests possible copy number expansion. Gene duplication can occur for various reasons, including loss-of-function leading to pseudogenes, life stage-specific functions, overlapping functions, neo-functionalization, or the production of multiple transcripts. However, RNA transcripts for both *Ld*α-SNAP genes exist in all *Leishmania* life forms, indicates they are neither pseudogenes nor stage-specific. While multiple paralogs arise from a common ancestral gene (67), their diversification through evolution may result in structural divergences of gene products. In *Plasmodium*, CLAG protein paralogs form nutrient uptake channels in the erythrocyte membrane. Although all the CLAG genes are transcribed simultaneously, their paralogs mainly differ in the loop size exposed to plasma, leading to varied responses during extracellular protease treatment (69). To assess if the two *Ld*α-SNAPs are subfunctional or neofunctional, we examined the conservation of their canonical structural attributes, as structural divergence may indicate evolutionary functional selection. The crystal structure of *Sc*Se17 shows 14 α-helices, forming an N-terminal twisted sheet and a C-terminal globular bundle, crucial for SNARE and NSF interaction. One edge of the twisted sheet was extended further than the other, conferring distinct concave and convex surfaces, a characteristic conserved across eukaryotic α-SNAP (36). The conservation of all these structural features of canonical α-SNAP within *Ld*α-SNAPs suggests that these paralogs might perform an overlapping function similar to *Sc*Sec17. Besides structural similarities, the conservation of almost all the SNARE (except for the lysine to glutamate (E151) substitution in *Ld*α-SNAP2) and membrane-interacting residues in both *Ld*α-SNAPs, implying their possible role in cis-SNARE disassembly, analogous to canonical eukaryotic α-SNAP. Nevertheless, the varying capabilities of *Ld*α-SNAPs to complement the *Sc*Sec17 function, highlight their importance in studying other functional attributes.

Functional diversification in Ldα*-SNAPs is achieved by substituting an N-terminally located phosphorylatable-serine*

A single nucleotide substitution during gene duplication can lead to neofunction that benefits the organism (70). For instance, the conversion of lysine to asparagine in the transcriptional regulator teosinte glume architecture 1 (tga1) changes its function from an activator to a repressor, transforming solid teosinte to naked maize kernels (71). Phosphorylation of serine-6 in *Tg*α-SNAP is crucial for regulating secretory traffic, biogenesis of Golgi, and other apicomplexan-specific organelles (23). The conservation of this phosphorylatable-serine-6 in *Ld*α-SNAP1 along with its substitution by aspartate in *Ld*α-SNAP2 could be the reason behind the varying capability of the two *Ld*α-SNAPs to substitute *Sc*Sec17 function. This assumption is supported by the observation that when aspartate-6 in *Ld*α-SNAP2 is replaced with serine, its capability to functionally complement *Sc*Sec17 is restored, indicating that either *Ld*α-SNAP2 may have lost this residue or serine was later incorporated in *Ld*α-SNAP1 by replacing alanine during evolution to meet the specific functional needs of *Leishmania*. This also rules out the hypothesis of *Leishmania* keeping these paralogs for the need for an ample amount of α-SNAP transcript (72). Moreover, we found that both *Ld*α-SNAPs can complement *Sc*Sec17 after phosphomimetic substitution of serine-6 (in *Ld*α-SNAP1) and aspartate-6 (in *Ld*α-SNAP2) with glutamate. This emphasizes the importance of residue position, charge, and structure in the functionality of α-SNAP. This result is echoed in a previous report, which showed that substituting serine-90 with glutamic acid in bovine prolactin mimics phosphorylation, leading to a mutated prolactin that exhibits biological activity similar to that of its wild-type counterparts (50).

Phosphorylatable-serine at the N-terminus of α-SNAP is rarely found in trypanosomatida

Trypanosomatid genomes frequently exhibit duplications, as seen with the α-SNAP gene in *Leishmania*, which likely arose from a divergent event rather than lateral gene transfer due to evolutionary forces (73). This assumption is supported by our phylogenetic tree topology, which shows that two α-SNAP sequences from reference trypanosomatid parasites evolved from a common ancestor before separating into clusters: one with Ldα-SNAP1 and the other with Ldα-SNAP2 (Fig. 7*A*, marked with solid and dashed bidirectional arrows). The phylogram also demonstrates that these genes evolved from a common ancestor through gene duplication and were subsequently diverged into two descendant groups. Each group may have acquired different regulatory pathways for more dedicated function within the same organism. This is exemplified by cysteine peptidases of parasitic protozoan, which serve distinct roles despite having identical sequences (74). In our sequence alignment of trypanosomatid α-SNAP orthologs clustered with *Ld*α-SNAP1, we identified the presence of phosphorylatable serine at position six only in *L. donovani* and *Porcisia hertigi* α-SNAPs (Fig. 7*B*). In contrast, other trypanosomatids contain either alanine or arginine at this position (Fig. 7*B*, marked with red box). This suggests that the incorporation of serine by these parasites occurs during evolution, which leads to pronounced functional specialization. This was also supported by the co-evolution of *Leishmania* and *P. hertigi* and the formation of a distinct clade from

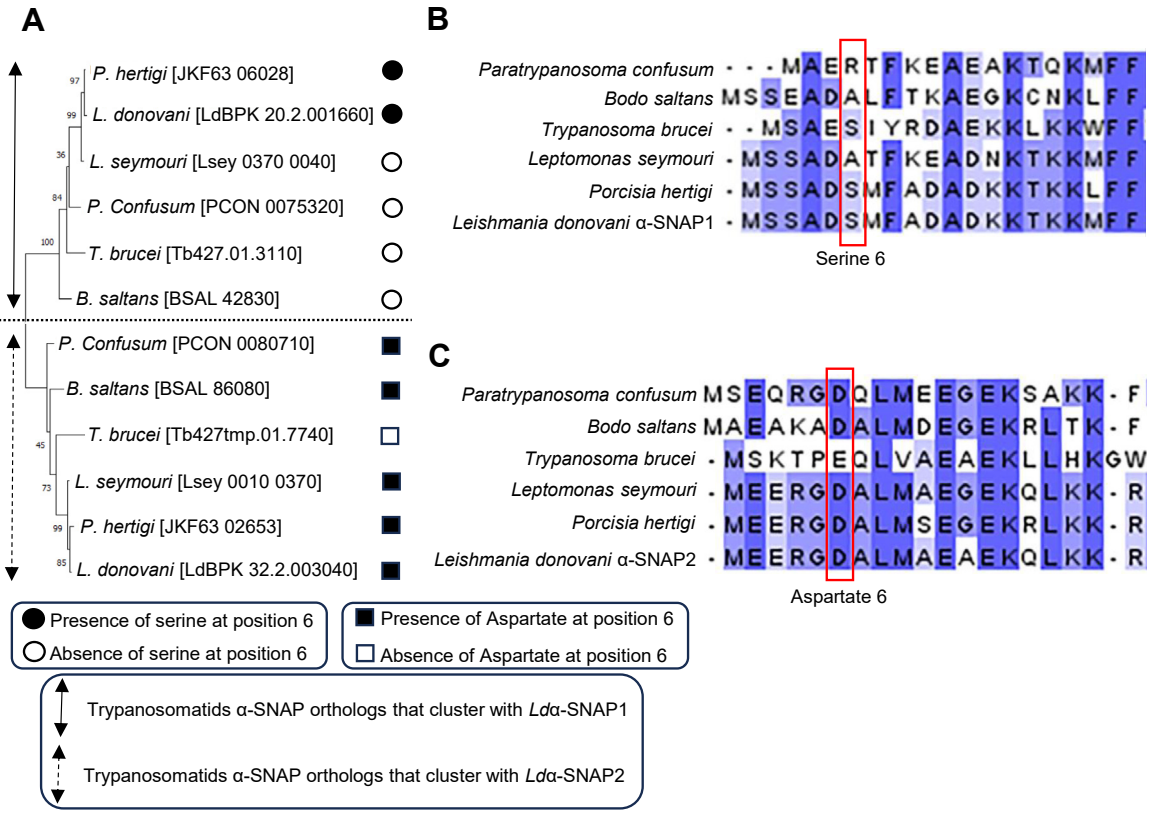

Figure 7. Phylogenetic analysis and sequence alignment of putative α-SNAP orthologs from diverse trypanosomatids. *A*, sequences of both α-SNAP paralogs from the parasites across the order trypanosomatida were used to reconstruct a maximum likelihood algorithm-based phylogenetic tree. The accession numbers of all the α-SNAP orthologs used in the study are listed in brackets next to the organism's name. The numerical value close to each node of the reconstructed tree indicates bootstrap values obtained from 100 replicates. The *closed and open circles* next to the accession number indicate the presence and absence of serine residue, respectively, at the sixth position in one of the α-SNAP paralogs of diverse trypanosomatids. Likewise, the *closed and open boxes* showed the presence and absence of aspartate at the same position as the other paralogs of the same organisms. The α-SNAP orthologs from diverse trypanosomatids, that clustered with: *B*, *Leishmania donovani* α-SNAP1, and, (*C*) *Ld*α-SNAP2, in the phylogenetic tree, were aligned separately in CLUSTALW. The conserved residues (serine or aspartate) at the sixth position of both the alignments were marked with *red boxes*.

the most common ancestor in the phylogenetic tree (Fig. 7*A*) (75). Notably, phosphorylated α-SNAP has been reported to bind the cis-SNARE complex 10 times weaker than the wild-type (17), indicating that serine-6-containing α-SNAP ortholog of *Leishmania* and *Porcisia* may perform SNARE and NSF-independent, non-canonical function. Conversely, the preserved aspartate residue at the sixth position of *Ld*α-SNAP2 and its corresponding orthologs of other trypanosomatids (Fig. 7*C*) suggest a likely conservation of its function within these parasites.

Subfunctions and acquired parasite-specific neofunction by Ldα*-SNAP paralogs are crucial for the parasite's survival and transmission*

The identified *Ld*α-SNAPs are paralogous genes that exhibit distinct abilities to substitute *Sc*Sec17 function as well as differing subcellular distributions. *Ld*α-SNAP1 is located at the FP, endosomal compartment, and flagellum, while *Ld*α-SNAP2 is found in the ER. For instance, zebrafish possess two transcription factors, engrailed-1 and engrailed-1b, which arise from chromosomal duplication. Engrailed-1 is expressed in the pectoral appendage bud, while engrailed-1b is expressed in neurons of the hindbrain and spinal cord. (76). *Ld*α-SNAP1 appears to be involved in cis-SNARE disassembly at the FP, as evidenced by its interaction with *Ld*NSF, the presence of *Ld*NSF and *Lm*Qa SNARE *LmjF*28.1470 (the two cognate binding partners of α-SNAP) at the leishmanial FP, as well as its ability to complement *Sc*Sec17 function. In contrast, *Ld*α-SNAP2 localized in the ER, where no Qa-SNAREs or NSF have yet been reported, and it cannot substitute for *Sc*Sec17 functionally. This suggests that *Ld*α-SNAP2 may serve a non-canonical function, specific to *Leishmania*. The non-canonical functions of α-SNAP have been observed in mammals, which include regulation of store-operated Ca^{2+} entry at the ER-PM junction in coordination with Orai1 and Stim1, maintaining the morphology of the ER in association with an ER-located SNARE, BNIP1, and suppressing apoptosis (24, 77). The presence of *Ld*α-SNAP1 in the endosomal compartment, alongside the small GTPase Rab5a (a key regulator of endosomal trafficking), and Rab11 (known for its role in transporting materials from early endosomes to the Golgi), suggests that *Ld*α-SNAP1 is likely involved in endosome-endosome fusion and cargo recycling in *Leishmania* (51, 52, 78, 79). This assumption is bolstered by the localization of the leishmanial SNARE component LmjF19.0120 in late endosomes (14). Additionally, the *Ld*α-SNAP1's presence at the *Leishmania* flagellum, where several membrane-bound sensors have been reported, indicates

a novel role of this protein in sensing environmental cues (54). Furthermore, a recent report has shown that leishmanial kinetoplastid-associated proteins (KIAP) share a similar distribution with *Ld*α-SNAP1, implying that the latter may assist the parasite in adhering to the stomodeal valve of the infected sandfly's hindgut, which is critical for parasite survival and transmission (53).

The FP of *Leishmania* is well-known for releasing virulence factors that help the parasite evade the host's defense mechanism (5). One such secretory protein is the metalloprotease GP63, which is transported from ER through various membrane-enclosed compartments of secretory routes before being released into the extracellular milieu from the FP and cell surface (5, 60, 65). Overlapping signals of GP63 and *Ld*α-SNAP1 at the FP, alongside the accumulation of GP63 in the cytosol following *Ld*α-SNAP1$_{(L281A)}$ overexpression, suggest that *Ld*α-SNAP1 promotes the fusion of GP63-containing vesicles with the FP membrane for exocytosis. This is further supported by previous observations, where bromoenol lactone treatment or overexpression of dominant negative GTPase Sar1 in promastigotes blocks GP63 trafficking and exocytosis, accumulating GP63 in the cytosol (65, 80). Similar mislocalization of GP63 has been observed with *Ld*α-SNAP2$_{(L290A)}$ overexpression, indicating its possible role in GP63 trafficking from ER. Given that no SNAREs or NSF have been visualized/reported yet in the ER, *Ld*α-SNAP2 may possess an unconventional, parasite-specific function, which either directly or passively promotes the transport of GP63 from its site of synthesis (ER) to its site of release.

Overall, this study concludes that the expansion of the α-SNAP gene family in *Leishmania* is likely driven by the need for parasite-specific functions, in addition to the canonical functions that are essential for survival and pathogenicity. *Leishmania* retains one α-SNAP paralog (*i.e.*, *Ld*α-SNAP1) for its canonical, NSF and SNARE-dependent role in the fusion of GP63-containing vesicle to the FP for its subsequent exocytosis. Additionally, *Leishmania* maintains a second copy (*i.e.*, *Ld*α-SNAP2) that is thought to facilitate GP63 trafficking from ER to the cell surface and FP through an unconventional pathway. This indicates a subfunctionalization between the paralogs to release virulence factors extracellularly and evolutionary conservation of ancestral functions. Further investigation is necessary to elucidate *Ld*α-SNAP2's unconventional transport mechanism for GP63 release. Interestingly, the parasite uses a small fraction of *Ld*α-SNAP1 (probably post-translationally modified or Serine-6 phosphorylated) to execute an acquired neofunction in sensing environmental cues and/or possibly aiding the parasite's adhesion within the infected sandflies' hindgut. These observations suggest a strategic adaptation by *Leishmania* to survive and dwell within multiple hosts.

Experimental procedures

Bioinformatics analysis, sequence alignment, and secondary structure predictions

To explore α-SNAP orthologs in *L. donovani* and other parasitic protists, we used a well-characterized *S. cerevisiae* or yeast α-SNAP (*Sc*Sec17) protein sequence as a query for BLAST searches. These searches were conducted in Kinetoplastid Informatics Resources (https://tritrypdb.org) and the Eukaryotic Pathogen, Vector and Host Informatics Resources (https://veupathdb.org). We also retrieved α-SNAP sequences from various *L. donovani* strains and leishmanial species through BLAST search in the integrated kinetoplastid parasite database TriTrypDB. Additionally, α-SNAP sequences from multicellular eukaryotes were curated either from the NCBI database (https://www.ncbi.nlm.nih.gov) or the UniProt database (https://www.uniprot.org). To calculate the percentage identity of amino acids, we aligned the identified protein sequences using a pairwise sequence alignment tool, EMBOSS Needle (www.ebi.ac.uk/jdispatcher/psa/emboss_needle). Moreover, the individual *L. donovani* α-SNAP sequences were analyzed in the Pfam (Protein families database) (https://pfam.xfam.org) to determine the presence of characteristic domain(s) within these two proteins. The full sequences of *Ld*α-SNAPs and *Sc*Sec17 proteins were aligned by CLUSTALW, and visualized with Jalview (81, 82). The secondary structure predictions for *Ld*α-SNAPs were carried out in the I-TASSER (Iterative Threading ASSEmbly Refinement) server (https://zhanggroup.org/I-TASSER/), and the crystal structure of *Sc*Sec17 was sourced from Protein Data Bank (PDB Id: 1QQE) (https://www.wwpdb.org) (83). The secondary structural elements were marked onto the aligned α-SNAP sequences. The 3-dimensional automatic threading models of *Ld*α-SNAPs were generated based on *Sc*Sec17 crystal structure as a template in I-TASSER. Conserved SNARE-interacting residues in the thread models of *Ld*α-SNAP1 and *Ld*α-SNAP2 were marked using Pymol (84).

Parasite culture

L. donovani (MHOM/IN/1983/AG83 isolate) promastigotes were obtained from Prof. Amitabha Mukhopadhyay, Indian Institute of Technology Delhi. Wild-type promastigotes were routinely maintained in RPMI-1640 medium (pH 7.2) (Gibco, Thermo Fisher Scientific Inc) supplemented with 10% (v/v) heat-inactivated fetal bovine serum (Gibco, Thermo Fisher Scientific Inc), 50 μg/ml gentamicin (Himedia) and 100 μg/ml penicillin-streptomycin mix (Gibco, Thermo Fisher Scientific Inc) for 4 days at 24 °C. Briefly, 5×10^5 cells were routinely inoculated in fresh medium and subcultured every 4 days intervals (85). All experiments were performed using mid-log phase promastigotes. To convert promastigotes to axenic amastigotes *in vitro*, we followed the methodology described by Jayanarayan and Dey, and Ephros *et al.* with minor modifications (86, 87). The late logarithmic phase promastigotes were transferred to fresh RPMI-1640 medium containing 25% (v/v) FBS in a T-25 cell culture flask and incubated for 16 to 24 h at 37 °C with 5% CO_2. After incubation, cells were pelleted by centrifugation at 1200*g* for 10 min at room temperature (RT), then resuspended in the RPMI-1640 medium supplemented with 10 mM Succinate/Tris (pH 5.5). Promastigotes were then incubated for 120 h at 37 °C with 5% CO_2. Under these conditions, promastigotes differentiated into amastigotes within 120 h.

Total RNA extraction and reverse transcription-PCR

The transcripts of *Ld*α-SNAP1 and *Ld*α-SNAP2 were analyzed *via* reverse transcription-PCR. Total RNA was extracted from promastigotes and amastigotes using Trizol (Ambion, Life Technologies) following the manufacturer's protocol. Each sample of promastigotes and amastigotes were pelleted and resuspended in 800 μl of Trizol. Next, 200 μl of chloroform (Thermo Fisher Scientific) was added to each sample, vortexed for 15 to 20 s, and centrifuged (in Sigma 2-16KL) at 12,000*g* for 10 min at 4 °C to allow phase separation. The upper aqueous phase was carefully collected in a fresh microcentrifuge tube, and 500 μl of isopropanol (Sisco Research Laboratories Pvt. Ltd) was added to this. The mixture was vortexed for another 15 to 20 s and incubated for 10 min at RT. Following incubation, the mixture was centrifuged for 10 min at 12,000*g* at 4 °C. The RNA pellet was then washed with 75% ethanol by centrifugation at 7500*g* at 4 °C, dried at RT for 10 min, and dissolved in 20 to 30 μl of nuclease-free water (Himedia). The concentration of the RNA samples from both promastigotes and amastigotes was measured using a nanophotometer (Implen Inc) and contaminating genomic DNA was removed by DNase I (NEB) treatment for 15 min at 37 °C. Subsequently, 2 μg of purified mRNA was converted into complementary DNA (cDNA) using the iScript cDNA synthesis kit (Bio-Rad Laboratories) following the manufacturer's instructions. PCR amplifications were performed using gene-specific primers and cDNA as templates, along with Phusion High-fidelity DNA Polymerase (Thermo Scientific) to detect the expression of *Ld*α-SNAP genes and the control genes. The primer pairs (listed in Table S1) used in this study were designed against the unique region of leishmanial genes *viz. Ld*α-SNAP1, *Ld*α-SNAP2, promastigote-specific Receptor-type adenylate cyclase-A (racA), amastigote-specific A2, and housekeeping genes 18S rRNA and 40S ribosomal protein S8 (37–41).

Yeast culture

Wild-type yeast *S. cerevisiae* (strain MATα: *his3Δ1 leu2Δ0 lys2Δ0 ura3Δ0*) (a kind gift from Prof. Alok Kumar Mondal, School of Life Sciences, Jawaharlal Nehru University) and temperature-sensitive mutant (ts-mutant) yeast strain RSY269 (MATα *ura3-52 his4-619 sec17–1*) (a kind gift from Prof Randy Schekman, UC, Berkeley) cells were grown in YEPD medium, containing 2% dextrose (Sisco Research Laboratories Pvt. Ltd), 2% peptone (Sisco Research Laboratories Pvt. Ltd) and 1% yeast extract (Himedia), at a permissive temperature of 30 °C. Whereas, the yeast transformants were grown in synthetic complete medium (YCM), containing the complete supplement mixture w/o uracil (YCM Ura d/o) (Himedia), yeast nitrogen base without amino acids (Sigma), and 2% dextrose, at both permissive (30 °C) and non-permissive (37 °C) temperatures.

Functional complementation

To study the functional complementation of *Ld*α-SNAP1 and *Ld*α-SNAP2 in yeast, the ts-mutant yeast strain RSY269 was used. The RSY269 strain harbors a mutation in the *SEC17* gene (*sec17–1*) of the yeast vesicular trafficking pathway (46). The chromosomal sequences of α-SNAP genes from both wild-type yeast (MATα) and *Leishmania* (AG83) were first PCR-amplified using the primers listed in Table S1 and then individually cloned under the control of a strong constitutive promoter, glyceraldehyde 3-phosphate dehydrogenase (GPD), into a 2μ plasmid, p426GPD (ATCC 87361), having *URA3* as the yeast selectable marker gene. The resulting constructs were individually transformed into RSY269 and plated onto YCM Ura d/o plates. Transformants were allowed to grow overnight at 30 °C, and colonies that grew on YCM Ura d/o plates were selected for functional complementation study. Next, colonies from each transformant (p426GPD-*SEC17* in RSY269, p426GPD-α-SNAP1 in RSY269, and p426GPD-α-SNAP2 in RSY269) were inoculated in liquid YCM Ura d/o medium and grown overnight at 30 °C with shaking. The resulting cultures were serially diluted to different desired concentrations and spotted onto YCM Ura d/o plates. The plates were then incubated at both permissive (30 °C) and non-permissive temperatures (37 °C) for 2 days to evaluate the extent of *Ld*α-SNAPs' complementation in comparison to corresponding *Sc*Sec17.

Phosphorylation prediction, site-directed mutagenesis, and functional complementation in yeast hypomorph

The sequence and structure-based prediction of serine phosphorylation sites was conducted using the entire amino acid sequences of both *Ld*α-SNAPs and *Sc*Sec17 (Table S3) through the NetPhos 3.1 server (https://services.healthtech.dtu.dk/services/NetPhos-3.1/).

Point mutations were introduced into the constructs p426GPD-*SEC17*, p426GPD-α-SNAP1, and p426GPD-α-SNAP2 using site-directed mutagenesis (SDM) PCR with KOD Hot Start DNA Polymerase (Sigma). The primer pairs (listed in Table S1) used in PCR contained the desired mutations at precise locations. The standard 20 μl SDM PCR mixture included: 2 μl of 10× buffer for KOD Hot Start DNA Polymerase, 1.2 μl of 25 mM MgSO4, 1 μl of 2 mM of dNTP mixture, 0.5 μl each of forward and reverse primer from 1 μM stock, 0.4 μl of 1 U/μl KOD Hot Start DNA Polymerase, 0.4 μl of 100% DMSO (Thermo Fisher Scientific Inc) and 0.3 μl of 100 ng/μl of the template DNA. The PCR was performed following the manufacturer's protocol with minor modifications: initial denaturation at 95 °C for 5 min, second denaturation at 95 °C for 40 s, annealing at 55 to 60 °C (depending on the primer pairs) for 45 s, and extension at 70 °C at 4 min 30 s followed by a final extension at 70 °C for 8 min. The cycles of denaturation, annealing, and primer extension stages were repeated for 20 cycles. After PCR amplification, the SDM PCR products were subjected to agarose gel electrophoresis and visualized under a UV transilluminator. Next, to eliminate the template plasmid from the amplified SDM PCR products, digestion with DpnI (NEB) was done at 37 °C for 2 h, followed by inactivation of DpnI enzyme at 80 °C for 20 min. The DpnI-digested SDM PCR products were then transformed into

DH-5α super-competent cells and plated on Luria broth (LB) agar (Himedia) plates containing 100 μg/ml ampicillin (Himedia). The presence of the desired mutations in the α-SNAPs were confirmed by Sanger sequencing (Eurofins India). The constructs containing mutant α-SNAPs were subsequently transformed individually into RSY269, and functional complementation was performed as previously described.

Similarly, the substitution of C-terminal leucine with alanine in wild-type *Ld*α-SNAP1 and *Ld*α-SNAP2 was carried out using the primer pairs (listed in Table S1) that contained the desired mutation following the methodology described above. The incorporation of the desired mutations at a precise location in both *Ld*α-SNAP genes (*Ld*α-SNAP1$_{(L281A)}$ and *Ld*α-SNAP2$_{(L290A)}$) was confirmed through Sanger sequencing.

Plasmid, antibodies, and organelle tracking dyes

To visualize the intracellular distribution of episomally expressed Green Fluorescent Protein (GFP)-tagged α-SNAP2 in promastigotes, full-length α-SNAP (Ld_3040) was PCR amplified using the primer pair listed in Table S1. This was then cloned into the pXG-GFP^{+2} vector (a kind gift from Prof. Stephen M. Beverley, Washington University, St Louis) in-frame with GFP ORF, placing GFP at the N-terminus of *Ld*α-SNAP2 (88). For immunolocalization of *Ld*α-SNAP1, a custom polyclonal antibody was raised (by Bio Bharati Life Science) in rabbits using full-length *Ld*α-SNAP1 protein as an immunogen. The antigenic determinants of both *Ld*α-SNAPs were identified by analyzing their complete amino acid sequences using the method previously described by Kolaskar and Tongaonkar (89) (Table S4). Additionally, to monitor the localization of NSF and GP63 within promastigotes, their respective primary antibodies, anti-NSF rabbit polyclonal antibody (Invitrogen, Thermo Fisher Scientific Inc) and *Leishmania* Gp63 mouse monoclonal antibody (Thermo Fisher Scientific Inc) were used, respectively. The antigen-primary antibody complexes formed within the promastigotes were visualized under a confocal microscope using suitable fluorophore-conjugated secondary antibodies. These included Goat anti-rabbit IgG Alexa Fluor 488 conjugate (Cell Signaling Technology Inc) and Goat anti-mouse IgG Alexa Fluor 555 conjugate (Invitrogen, Thermo Fisher Scientific Inc), applied according to the specific requirements. Finally, the ER and the Golgi in live promastigotes were stained with ER-Tracker Blue-White DPX (Molecular probes, Thermo Fisher Scientific Inc) (A kind gift from Prof. Aditya Mittal, Indian Institute of Technology Delhi) and Bodipy -TR Ceramide (Invitrogen, Thermo Fisher Scientific Inc), respectively, following the manufacturer's instructions.

Electroporation in Leishmania

Electroporation was performed in promastigotes, as previously described (90, 91). Briefly, 5 × 10^7 promastigotes were pelleted by centrifugation at 1200*g* for 10 min at 4 °C. The resulting cell pellet was then washed twice with 1× Phosphate-buffered saline (PBS) and resuspended in an ice-cold electroporation buffer consisting of 21 mM HEPES (Himedia), 137 mM NaCl (Merck), 5 mM KCl (Sigma), 0.7 mM NaH_2PO_4 (Sigma), 6 mM glucose (pH 7.4) to achieve a final concentration of 1 × 10^8 cells/ml. Next, the resuspended cells were placed in a pre-chilled 4 mm (0.4 cm) gap sterile electroporation cuvette (Bio-Rad Laboratories) and incubated on ice for 10 min. Following this, 10 to 20 μg pre-chilled plasmids (Wild-type: pXG-GFP^{+2}-*Ld*α-SNAP2, and Mutants: pXG-GFP^{+2}-*Ld*α-SNAP1$_{(L281A)}$ and pXG-GFP^{+2}-*Ld*α-SNAP2$_{(L290A)}$) were separately added to each cuvette and mixed thoroughly. Electroporation was then performed using a Bio-Rad Gene Pulser, applying two pulses at 1500 V, with a capacitance of 25 μF, and a resistance of 200 Ω, allowing 10 s pause between the pulses. Next, the electroporated cells were incubated on ice for additional 10 min and transferred to a 25 mm cell culture flask containing freshly prepared drug-free RPMI-1640 medium. The cells were allowed to recover by incubating the flask on its side for 30 h at 24 °C. Finally, transfectants were selected and maintained in 100 μg/ml G418 sulfate (Gold Biotechnology) antibiotic. The intracellular expression of GFP-tagged *Ld*α-SNAP2 was analyzed by WB with anti-GFP mouse monoclonal antibody (Invitrogen, Thermo Fisher Scientific Inc).

Preparation of whole-cell lysate, western immunoblotting, and stripping

The whole-cell lysate of promastigotes was prepared as described by Prasad *et al.* (85). Wild-type or transfected promastigotes were pelleted by centrifugation at 1200*g* for 10 min at 4 °C, and washed thrice with ice-cold 10 mM PBS (pH 7.4). The pellet was resuspended in lysis buffer containing 20 mM Tris-Cl (pH 7.0), 150 mM NaCl, 1 mM EDTA (Sigma), 0.1% Triton X-100 (Sigma), 2 mM phenylmethylsulfonyl fluoride (PMSF) (Sisco Research Laboratories Pvt. Ltd), 10 μg/ml each of leupeptin (Sigma) and aprotinin (Sigma). Cell lysis was allowed to proceed for 30 min at 4 °C,after which, the supernatant was collected by centrifugation at 16000*g* for 15 min, and the protein concentration in whole-cell lysate was estimated using the bicinchoninic acid (BCA) (Sigma) method in iMark Microplate Absorbance Reader (Bio-Rad Laboratories) with bovine serum albumin (BSA) as standard (92). For western immunoblotting, lysates containing equal concentrations of proteins (25 μg) were heated with 1× Laemmli sample buffer (containing 62.5 mM Tris-Cl pH 6.7, 10% glycerol (v/v) (Sisco Research Laboratories), 2% SDS (w/v) (Sigma), 0.003% Bromophenol blue (w/v) (Sisco Research Laboratories) and 14.3 M β-mercaptoethanol (Sigma) at 90 °C for 7 min. The samples were then resolved on a 7% SDS PAGE, and transferred to a nitrocellulose membrane (mdi Membrane Technologies Inc). Next, the membrane was blocked with blocking solution of 5% BSA and 5% FBS before being serially probed with primary antibodies, namely anti-α-SNAP1 rabbit antibody, anti-NSF rabbit antibody, anti-GFP mouse monoclonal antibody, and anti-GAPDH mouse antibody or anti-GAPDH rabbit antibody (Cell Signaling Technology) for 12 to 16 h at 4 °C. This was followed by incubation with corresponding secondary antibodies *e.g.* goat anti-rabbit IgG HRP conjugate

(Cell Signaling Technology) and horse anti-mouse IgG HRP conjugate (Cell Signaling Technology) for 2 h at RT. Protein bands were visualized with Immobilon western chemiluminescent HRP substrate (Millipore, Merck) using the ImageQuant LAS500 system (GE Healthcare). To remove the antibodies from the membrane, the stripping technique was used. The blots were incubated at 50 °C with shaking for 30 min in a stripping buffer composed of 62.5 M Tris-Cl pH 6.8, 2% SDS, and 100 mM β-mercaptoethanol, followed by several washes with Tris Buffered Saline-Tween 20 (TBST) (93). Subsequently, the membrane was blocked again and reprobed with a new set of primary and secondary antibodies, as mentioned above.

Live and fixed-cell immunofluorescence and confocal microscopy

Live-cell IF in promastigotes was performed as described by Kapur *et al.* (94). Briefly, 1 × 10^7 wild-type or transfected promastigotes were pelleted by centrifugation at 1200*g* for 10 min, washed with 1× PBS, and resuspended in 50 µl of IF buffer (IFB) containing 1× PBS, 1% Glucose and 10% FBS. Cells were then incubated on ice for 30 min with a primary antibody diluted 1:50 in IFB. Cells were washed thrice with 1 ml of chilled IFB before resuspending in 100 µl IFB containing the fluorochrome-coupled secondary antibody and incubated at 4 °C for 30 min with occasional mixing. Following incubation, cells were washed thrice with ice-cold IFB and resuspended in 200 to 300 µl of IFB. An 8 µl aliquot of the cell suspension was overlayed onto a poly L-Lysine (EMD Millipore Corp) coated coverslip, mounted on a glass slide using ProLong Diamond Antifade Mountant (Invitrogen, Thermo Fisher Scientific Inc) reagent, and observed under the 100× oil immersion objective lens of FLUOVIEW FV1200 Confocal Laser Scanning microscope (Olympus Life Science, IX83). For dual labeling of *Ld*NSF or *Ld*α-SNAP1 with a Golgi staining dye, promastigotes were first incubated with 5 µM Bodipy -TR Ceramide in culture medium (RPMI1640) supplemented with 1.8% defatted BSA (Gold Biotechnology) for 48 h at 24 °C (95). After incubation, cells were placed on ice for 30 min and then washed thrice with 1 ml of chilled IFB. Next, live-cell IF was carried out in the dark on these Golgi-stained promastigotes, as mentioned above, with either anti-NSF rabbit polyclonal or anti-α-SNAP1 rabbit polyclonal primary antibody along with their corresponding goat anti-rabbit IgG Alexa Fluor 488 coupled secondary antibody. To determine the subcellular localization of GFP-tagged α-SNAP2 at the ER, promastigotes expressing the GFP-tagged-α-SNAP2 were washed thrice with IFB, treated with 1 µM ER-Tracker Blue-White DPX dye in IFB and incubated at 37 °C for 30 min. After incubation, cells were washed with IFB to remove the staining solution and visualized under the confocal microscope after being mounted on the glass slide.

For fixed-cell IF, promastigotes were harvested by centrifugation at 1200*g* for 10 min with or without preincubation at 37 °C for 4 h. Cells were washed thrice by centrifugation at the same speed for 10 min using 1× PBS. The cell pellet was resuspended in a fixing solution, of 4% formaldehyde (v/v) (Thermo Fisher Scientific India), and incubated at RT for 20 min. After fixing, cells were harvested by centrifugation and resuspended in 0.1 M glycine (Himedia) for 5 min at RT. Subsequently, the promastigotes were washed once with ice-cold 1× PBS and permeabilized with 0.1% Triton X-100 for 7 min on ice. Cells were again washed with 1× PBS and blocked with 2% BSA (Himedia) for 2 h at RT with shaking. For immunolabeling, promastigotes expressing *Ld*α-SNAP1, GFP-*Ld*α-SNAP2, GFP-*Ld*α-SNAP1$_{(L281A)}$ and GFP-*Ld*α-SNAP2$_{(L290A)}$, and *Ld*GP63 proteins, were incubated overnight at 4 °C with their respective antisera (anti-α-SNAP1, anti-GFP, and anti-GP63) either individually or in combination with gentle shaking. The next day, cells were washed thrice with 1× PBS by centrifugation at 1200*g* for 10 min and then incubated with Alexa Fluor 488 or Alexa Fluor 555 conjugated secondary antibodies at a dilution ratio of 1:400 for 2 h at RT with shaking. After washing thrice with 1× PBS, cells were resuspended in the required volume (250 to 300 µl) of 1× PBS and mounted using ProLong Diamond Antifade Mountant on a glass slide. Samples were imaged under the confocal microscope. The microscopic images were assembled with Adobe Photoshop and Adobe Illustrator. Each immunofluorescence confocal microscopy experiment was repeated thrice with each biological replicate with three technical replicates.

Colocalization analysis

Colocalization by line scan analysis was carried out using the fluorescent intensities of two fluorophores as previously described (96–98). The fluorescent intensity (Y-axis) *versus* the distance along the line (X-axis), drawn on the image, were plotted using ImageJ2 (99).

Statistical analysis

The Pearson correlation coefficient value (r) for each colocalization experiment was calculated using the ImageJ2 plugin JACoP.

Immunoprecipitation (IP)

To perform IP, we followed our lab protocol (100). The whole-cell lysates were prepared in lysis buffer (20 mM Tris-Cl (pH 7.0), 150 mM NaCl, 1 mM EDTA, 0.1% Triton X-100, 2 mM PMSF, 10 µg/ml each of leupeptin and aprotinin) as previously described. The protein concentration in whole-cell lysate was estimated using the bicinchoninic acid method (101). A total of 500 µg protein lysate was mixed with anti-α-SNAP1 antibody (1:100 dilution) and incubated overnight at 4 °C in a Rotospin Test Tube Rotator Disk (Tarsons) for end-to-end mixing. The next day, protein A/G Plus Agarose beads (Santa Cruz Biotechnology), lysis buffer, and protease inhibitors were added to this and incubated for another 4 h at 4 °C in a rotator mixer. The whole-cell lysate incubated with only A/G beads was used as a negative control for the experiment. After incubation, the mixer (Cell-lysate, anti-α-SNAP1 antibody, A/G beads, lysis buffer, and protease inhibitors) was centrifuged at 5000 rpm for 5 min, and the supernatant was discarded. The beads were carefully washed thrice with lysis

buffer containing protease inhibitors to remove the unbound antibodies and proteins. Finally, 1× Laemmli sample buffer was added to the beads and heated for 7 min at 90 °C. The eluted or immunoprecipitated proteins were loaded and resolved on 7% SDS-PAGE and visualized by Western immunoblotting with anti-NSF and anti-α-SNAP1 primary antibodies along with their corresponding anti-rabbit HRP-conjugated secondary antibody, following the stripping and reprobing protocol.

Phylogenetic analysis

The sequences of both α-SNAP paralogs of the selected trypanosomatids were curated by BLAST search in the TriTrypDB database. Alignment and reconstruction of the maximum likelihood tree of the curated α-SNAP sequences were performed in Jalview and Mega 11, respectively, with 100 bootstrap replicates (102).

Data availability

All the raw data are deposited as a separate file named "Supporting information (Not for publication)" with this manuscript. All the data related to this manuscript are available from the corresponding author upon reasonable request.

Supporting information—This article contains supporting information.

Acknowledgments—We are grateful to the Indian Institute of Technology-Delhi for their support. We acknowledge Prof. Chinmay Kumar Mukhopadhyay (Special Centre for Molecular Medicine, Jawaharlal Nehru University, Delhi) for his valuable suggestion in the yeast complementation study. We want to thank Prof. Randy Schekman (University of California, Berkeley) and Prof. Alok Kumar Mondal (School of Life Sciences, Jawaharlal Nehru University, Delhi) for helping us by providing the yeast strains RSY269 and wild-type *Saccharomyces cerevisiae* (Matα), respectively. We thank Prof. Stephen M. Beverley (Washington University, St Louis) for providing the pXG-GFP^{+2} empty vector backbone. We are grateful to the Central Research Facility (CRF) of the Indian Institute of Technology-Delhi for the Confocal Microscopy facility.

Author contributions—S. P. D. and C. S.D. methodology; S. P. D. data curation; S. P. D. data analysis; S. P. D. writing original draft; S. P. D. approved final version of the manuscript; C. S. D. writing, review & editing; C. S. D. supervision; C. S. D. resources; C. S. D. project administration; C. S. D. funding acquisition; S. P. D. and C. S. D. conceptualization and investigation.

Funding and additional information—S. P. D. received fellowship support from the Research Associateship programme of the Council of Scientific and Industrial Research (CSIR), Government of India (File No. 09/0086(11807)/2021-EMR-I).

Conflict of interest—The authors declare that they have no conflicts of interest with the contents of this article.

Abbreviations—The abbreviations used are: α-SNAP, α-Soluble NSF Attachment Protein; ER, Endoplasmic reticulum; FP, Flagellar pocket; GFP, Green fluorescent protein; GPD, Glyceraldehyde 3-phosphate dehydrogenase; GP63, Glycoprotein 63; IF, Immunofluorescence; IFB, Immunofluorescence buffer; IP, Immunoprecipitation; I-TASSER, Iterative Threading ASSEmbly Refinement; KIAP, Kinetoplastid-associated proteins; *Ld*, *Leishmania donovani*; MIL, Membrane-interacting loop; MSA, Multiple sequence alignment; NSF, N-ethylmaleimide-sensitive factor; PM, Plasma membrane; PDB, Protein Data Bank; Sc, *Saccharomyces cerevisiae*; SDM, Site-directed mutagenesis; SNARE, Soluble NSF Attachment protein REceptor; *Tg*, *Toxoplasma gondii*; Tga1, Teosinte glume architecture 1; YCM, Yeast complete medium; YEPD, Yeast Extract Peptone Dextrose.

References

1. Sunter, J., and Gull, K. (2017) Shape, form, function and Leishmania pathogenicity: from textbook descriptions to biological understanding. *Open Biol.* **7**, 170165
2. Bates, P. A., and Rogers, M. E. (2004) New insights into the developmental biology and transmission mechanisms of Leishmania. *Curr. Mol. Med.* **4**, 601–609
3. Gupta, A. K., Das, S., Kamran, M., Ejazi, S. A., and Ali, N. (2022) The pathogenicity and virulence of Leishmania - interplay of virulence factors with host defenses. *Virulence* **13**, 903–935
4. Isnard, A., Shio, M. T., and Olivier, M. (2012) Impact of Leishmania metalloprotease GP63 on macrophage signaling. *Front. Cell Infect. Microbiol.* **2**, 72
5. McGwire, B. S., O'Connell, W. A., Chang, K.-P., and Engman, D. M. (2002) Extracellular release of the glycosylphosphatidylinositol (GPI)-linked Leishmania surface metalloprotease, gp63, is independent of GPI phospholipolysis: implications for parasite virulence. *J. Biol. Chem.* **277**, 8802–8809
6. Silverman, J. M., Clos, J., de'Oliveira, C. C., Shirvani, O., Fang, Y., Wang, C., *et al.* (2010) An exosome-based secretion pathway is responsible for protein export from Leishmania and communication with macrophages. *J. Cell Sci.* **123**, 842–852
7. Block, M. R., Glick, B. S., Wilcox, C. A., Wieland, F. T., and Rothman, J. E. (1988) Purification of an N-ethylmaleimide-sensitive protein catalyzing vesicular transport. *Proc. Natl. Acad. Sci. U. S. A.* **85**, 7852–7856
8. Malhotra, V., Orci, L., Glick, B. S., Block, M. R., and Rothman, J. E. (1988) Role of an N-ethylmaleimide-sensitive transport component in promoting fusion of transport vesicles with cisternae of the Golgi stack. *Cell* **54**, 221–227
9. Weidman, P. J., Melançon, P., Block, M. R., and Rothman, J. E. (1989) Binding of an N-ethylmaleimide-sensitive fusion protein to Golgi membranes requires both a soluble protein(s) and an integral membrane receptor. *J. Cell Biol.* **108**, 1589–1596
10. Stenbeck, G. (1998) Soluble NSF-attachment proteins. *Int. J. Biochem. Cell Biol.* **30**, 573–577
11. Clary, D. O., Griff, I. C., and Rothman, J. E. (1990) SNAPs, a family of NSF attachment proteins involved in intracellular membrane fusion in animals and yeast. *Cell* **61**, 709–721
12. Datta, S. P., Jana, K., Mondal, A., Ganguly, S., and Sarkar, S. (2018) Multiple paralogues of α-SNAP in Giardia lamblia exhibit independent subcellular localization and redistribution during encystation and stress. *Parasit. Vectors* **11**, 539
13. Perdomo, D., Aït-Ammar, N., Syan, S., Sachse, M., Jhingan, G. D., and Guillén, N. (2015) Cellular and proteomics analysis of the endomembrane system from the unicellular *Entamoeba histolytica*. *J. Proteomics* **112**, 125–140
14. Besteiro, S., Coombs, G. H., and Mottram, J. C. (2006) The SNARE protein family of Leishmania major. *BMC Genomics* **7**, 250
15. Tani, K., Shibata, M., Kawase, K., Kawashima, H., Hatsuzawa, K., Nagahama, M., *et al.* (2003) Mapping of functional domains of γ-SNAP. *J. Biol. Chem.* **278**, 13531–13538

16. Barnard, R. J. O., Morgan, A., and Burgoyne, R. D. (1997) Stimulation of NSF ATPase activity by α-SNAP is required for SNARE complex disassembly and exocytosis. *J. Cell Biol.* **139**, 875–883
17. Marz, K. E., Lauer, J. M., and Hanson, P. I. (2003) Defining the SNARE complex binding surface of α-SNAP: implications for SNARE complex disassembly. *J. Biol. Chem.* **278**, 27000–27008
18. Barszczewski, M., Chua, J. J., Stein, A., Winter, U., Heintzmann, R., Zilly, F. E., *et al.* (2008) A novel site of action for α-SNAP in the SNARE conformational cycle controlling membrane fusion. *Mol. Biol. Cell* **19**, 776–784
19. Söllner, T., Bennett, M. K., Whiteheart, S. W., Scheller, R. H., and Rothman, J. E. (1993) A protein assembly-disassembly pathway *in vitro* that may correspond to sequential steps of synaptic vesicle docking, activation, and fusion. *Cell* **75**, 409–418
20. Morgan, A., Dimaline, R., and Burgoyne, R. D. (1994) The ATPase activity of N-ethylmaleimide-sensitive fusion protein (NSF) is regulated by soluble NSF attachment proteins. *J. Biol. Chem.* **269**, 29347–29350
21. Baker, R. W., and Hughson, F. M. (2016) Chaperoning SNARE assembly and disassembly. *Nat. Rev. Mol. Cell Biol.* **17**, 465–479
22. Zhao, M., Wu, S., Zhou, Q., Vivona, S., Cipriano, D. J., Cheng, Y., *et al.* (2015) Mechanistic insights into the recycling machine of the SNARE complex. *Nature* **518**, 61–67
23. Stewart, R. J., Ferguson, D. J. P., Whitehead, L., Bradin, C. H., Wu, H. J., and Tonkin, C. J. (2016) Phosphorylation of αSNAP is required for secretory organelle biogenesis in Toxoplasma gondii. *Traffic Cph. Den.* **17**, 102–116
24. Miao, Y., Miner, C., Zhang, L., Hanson, P. I., Dani, A., and Vig, M. (2013) An essential and NSF independent role for α-SNAP in store-operated calcium entry. *eLife* **2**, e00802
25. Wang, L., and Brautigan, D. L. (2013) α-SNAP inhibits AMPK signaling to reduce mitochondrial biogenesis and dephosphorylates Thr172 in AMPKα *in vitro*. *Nat. Commun.* **4**, 1559
26. Naydenov, N. G., Feygin, A., Wang, L., and Ivanov, A. I. (2014) N-Ethylmaleimide-sensitive factor attachment protein α (αSNAP) regulates matrix adhesion and integrin processing in human epithelial cells. *J. Biol. Chem.* **289**, 2424–2439
27. Arcos, A., de Paola, M., Gianetti, D., Acuña, D., Velásquez, Z. D., Miró, M. P., *et al.* (2017) α-SNAP is expressed in mouse ovarian granulosa cells and plays a key role in folliculogenesis and female fertility. *Sci. Rep.* **7**, 11765
28. Barnard, R. J., Morgan, A., and Burgoyne, R. D. (1996) Domains of alpha-SNAP required for the stimulation of exocytosis and for N-ethylmalemide-sensitive fusion protein (NSF) binding and activation. *Mol. Biol. Cell* **7**, 693–701
29. Antonin, W., Holroyd, C., Fasshauer, D., Pabst, S., von Mollard, G. F., and Jahn, R. (2000) A SNARE complex mediating fusion of late endosomes defines conserved properties of SNARE structure and function. *EMBO J.* **19**, 6453
30. Kienle, N. (2010) *Phylogenetic Studies of the Vesicular Fusion Machinery*, PhD Thesis, Georg-August-Universität, Göttingen
31. Lakhssassi, N., Liu, S., Bekal, S., Zhou, Z., Colantonio, V., Lambert, K., *et al.* (2017) Characterization of the Soluble NSF Attachment Protein gene family identifies two members involved in additive resistance to a plant pathogen. *Sci. Rep.* **7**, 45226
32. Liu, F., Li, J.-P., Li, L.-S., Liu, Q., Li, S.-W., Song, M.-L., *et al.* (2021) The canonical α-SNAP is essential for gametophytic development in Arabidopsis. *PLoS Genet.* **17**, e1009505
33. Griff, I. C., Schekman, R., Rothman, J. E., and Kaiser, C. A. (1992) The yeast SEC17 gene product is functionally equivalent to mammalian alpha-SNAP protein. *J. Biol. Chem.* **267**, 12106–12115
34. Littleton, J. T. (2000) A genomic analysis of membrane trafficking and neurotransmitter release in Drosophila. *J. Cell Biol.* **150**, F77–F82
35. Tomes, C. N., De Blas, G. A., Michaut, M. A., Farré, E. V., Cherhitin, O., Visconti, P. E., *et al.* (2005) α-SNAP and NSF are required in a priming step during the human sperm acrosome reaction. *Mol. Hum. Reprod.* **11**, 43–51
36. Rice, L. M., and Brunger, A. T. (1999) Crystal structure of the vesicular transport protein Sec17: implications for SNAP function in SNARE complex disassembly. *Mol. Cell* **4**, 85–95
37. Badirzadeh, A., Taheri, T., Taslimi, Y., Abdossamadi, Z., Heidari-Kharaji, M., Gholami, E., *et al.* (2017) Arginase activity in pathogenic and non-pathogenic species of Leishmania parasites. *PLoS Negl. Trop. Dis.* **11**, e0005774
38. Adaui, V., Schnorbusch, K., Zimic, M., Gutiérrez, A., Decuypere, S., Vanaerschot, M., *et al.* (2011) Comparison of gene expression patterns among Leishmania braziliensis clinical isolates showing a different *in vitro* susceptibility to pentavalent antimony. *Parasitology* **138**, 183–193
39. Charest, H., Zhang, W. W., and Matlashewski, G. (1996) The developmental expression of Leishmania donovani A2 amastigote-specific genes is post-transcriptionally mediated and involves elements located in the 3'-untranslated region. *J. Biol. Chem.* **271**, 17081–17090
40. Charest, H., and Matlashewski, G. (1994) Developmental gene expression in Leishmania donovani: differential cloning and analysis of an amastigote-stage-specific gene. *Mol. Cell Biol.* **14**, 2975–2984
41. Sanchez, M. A., Zeoli, D., Klamo, E. M., Kavanaugh, M. P., and Landfear, S. M. (1995) A family of putative receptor-adenylate cyclases from Leishmania donovani. *J. Biol. Chem.* **270**, 17551–17558
42. Winter, U., Chen, X., and Fasshauer, D. (2009) A conserved membrane attachment site in α-SNAP facilitates *N*-Ethylmaleimide-sensitive factor (NSF)-driven SNARE complex disassembly. *J. Biol. Chem.* **284**, 31817–31826
43. Wimmer, C., Hohl, T. M., Hughes, C. A., Müller, S. A., Söllner, T. H., Engel, A., *et al.* (2001) Molecular mass, stoichiometry, and assembly of 20 S particles. *J. Biol. Chem.* **276**, 29091–29097
44. Alpizar-Sosa, E. A., Kumordzi, Y., Wei, W., Whitfield, P. D., Barrett, M. P., and Denny, P. W. (2022) Genome deletions to overcome the directed loss of gene function in Leishmania. *Front. Cell. Infect. Microbiol.* **12**, 988688
45. Schwartz, M. L., Nickerson, D. P., Lobingier, B. T., Plemel, R. L., Duan, M., Angers, C. G., *et al.* (2017) Sec17 (α-SNAP) and an SM-tethering complex regulate the outcome of SNARE zippering *in vitro* and *in vivo*. *eLife* **6**, e27396
46. Kaiser, C. A., and Schekman, R. (1990) Distinct sets of SEC genes govern transport vesicle formation and fusion early in the secretory pathway. *Cell* **61**, 723–733
47. Chothia, C., and Lesk, A. M. (1986) The relation between the divergence of sequence and structure in proteins. *EMBO J.* **5**, 823–826
48. Povolotskaya, I. S., and Kondrashov, F. A. (2010) Sequence space and the ongoing expansion of the protein universe. *Nature* **465**, 922–926
49. Chan, K.-F., Koukouravas, S., Yeo, J. Y., Koh, D. W.-S., and Gan, S. K.-E. (2020) Probability of change in life: amino acid changes in single nucleotide substitutions. *Biosystems* **193–194**, 104135
50. Maciejewski, P. M., Peterson, F. C., Anderson, P. J., and Brooks, C. L. (1995) Mutation of serine 90 to glutamic acid mimics phosphorylation of bovine prolactin. *J. Biol. Chem.* **270**, 27661–27665
51. Ambit, A., Woods, K. L., Cull, B., Coombs, G. H., and Mottram, J. C. (2011) Morphological events during the cell cycle of Leishmania major. *Eukaryot. Cell.* **10**, 1429–1438
52. Jeffries, T. R., Morgan, G. W., and Field, M. C. (2001) A developmentally regulated rab11 homologue in Trypanosoma brucei is involved in recycling processes. *J. Cell Sci.* **114**, 2617–2626
53. Yanase, R., Pruzinova, K., Owino, B. O., Rea, E., Moreira-Leite, F., Taniguchi, A., *et al.* (2024) Discovery of essential kinetoplastid-insect adhesion proteins and their function in Leishmania-sand fly interactions. *Nat. Commun.* **15**, 6960
54. Kelly, F. D., Yates, P. A., and Landfear, S. M. (2021) Nutrient sensing in Leishmania: flagellum and cytosol. *Mol. Microbiol.* **115**, 849–859
55. Povelones, M. L., Holmes, N. A., and Povelones, M. (2023) A sticky situation: when trypanosomatids attach to insect tissues. *PLoS Pathog.* **19**, e1011854
56. Halliday, C., Billington, K., Wang, Z., Madden, R., Dean, S., Sunter, J. D., *et al.* (2019) Cellular landmarks of *Trypanosoma brucei* and *Leishmania mexicana*. *Mol. Biochem. Parasitol.* **230**, 24–36
57. Ilgoutz, S. C., Mullin, K. A., Southwell, B. R., and McConville, M. J. (1999) Glycosylphosphatidylinositol biosynthetic enzymes are localized to a stable tubular subcompartment of the endoplasmic reticulum in Leishmania mexicana. *EMBO J.* **18**, 3643–3654

58. Hassani, K., Antoniak, E., Jardim, A., and Olivier, M. (2011) Temperature-induced protein secretion by Leishmania mexicana modulates macrophage signalling and function. *PLoS One* **6**, e18724
59. Hassani, K., Shio, M. T., Martel, C., Faubert, D., and Olivier, M. (2014) Absence of metalloprotease GP63 alters the protein content of Leishmania exosomes. *PLoS One* **9**, e95007
60. Santos, A. L. S., Branquinha, M. H., and D'Avila-Levy, C. M. (2006) The ubiquitous gp63-like metalloprotease from lower trypanosomatids: in the search for a function. *Acad. Bras. Cienc.* **78**, 687–714
61. He, P., Southard, R. C., Chen, D., Whiteheart, S. W., and Cooper, R. L. (1999) Role of alpha-SNAP in promoting efficient neurotransmission at the crayfish neuromuscular junction. *J. Neurophysiol.* **82**, 3406–3416
62. Field, M. C., and Carrington, M. (2009) The trypanosome flagellar pocket. *Nat. Rev. Microbiol.* **7**, 775–786
63. Langousis, G., and Hill, K. L. (2014) Motility and more: the flagellum of Trypanosoma brucei. *Nat. Rev. Microbiol.* **12**, 505–518
64. Isch, C., Majneri, P., Landrein, N., Pivovarova, Y., Lesigang, J., Lauruol, F., *et al.* (2021) Structural and functional studies of the first tripartite protein complex at the Trypanosoma brucei flagellar pocket collar. *PLoS Pathog.* **17**, e1009329
65. Parashar, S., and Mukhopadhyay, A. (2017) GTPase Sar1 regulates the trafficking and secretion of the virulence factor gp63 in Leishmania. *J. Biol. Chem.* **292**, 12111–12125
66. Cui, L., Li, H., Xi, Y., Hu, Q., Liu, H., Fan, J., *et al.* (2022) Vesicle trafficking and vesicle fusion: mechanisms, biological functions, and their implications for potential disease therapy. *Mol. Biomed.* **3**, 29
67. Dillman, A. R., Mortazavi, A., and Sternberg, P. W. (2012) Incorporating genomics into the toolkit of nematology. *J. Nematol.* **44**, 191–205
68. Ko, B. J., Lee, C., Kim, J., Rhie, A., Yoo, D. A., Howe, K., *et al.* (2022) Widespread false gene gains caused by duplication errors in genome assemblies. *Genome Biol.* **23**, 205
69. Gupta, A., Gonzalez-Chavez, Z., and Desai, S. A. (2024) Plasmodium falciparum CLAG paralogs all traffic to the host membrane but knockouts have distinct phenotypes. *Microorganisms* **12**, 1172
70. Fajardo, D., Saint Jean, R., and Lyons, P. J. (2023) Acquisition of new function through gene duplication in the metallocarboxypeptidase family. *Sci. Rep.* **13**, 2512
71. Wang, H., Studer, A. J., Zhao, Q., Meeley, R., and Doebley, J. F. (2015) Evidence that the origin of naked kernels during maize domestication was caused by a single amino acid substitution in tga1. *Genetics* **200**, 965–974
72. Pawar, H., Kulkarni, A., Dixit, T., Chaphekar, D., and Patole, M. S. (2014) A bioinformatics approach to reanalyze the genome annotation of kinetoplastid protozoan parasite *Leishmania donovani*. *Genomics* **104**, 554–561
73. Zinoviev, A., Akum, Y., Yahav, T., and Shapira, M. (2012) Gene duplication in trypanosomatids - two DED1 paralogs are functionally redundant and differentially expressed during the life cycle. *Mol. Biochem. Parasitol.* **185**, 127–136
74. Mottram, J. C., Helms, M. J., Coombs, G. H., and Sajid, M. (2003) Clan CD cysteine peptidases of parasitic protozoa. *Trends Parasitol.* **19**, 182–187
75. Steverding, D. (2017) The history of leishmaniasis. *Parasit. Vectors* **10**, 82
76. Force, A., Lynch, M., Pickett, F. B., Amores, A., Yan, Y. L., and Postlethwait, J. (1999) Preservation of duplicate genes by complementary, degenerative mutations. *Genetics* **151**, 1531–1545
77. Nakajima, K., Hirose, H., Taniguchi, M., Kurashina, H., Arasaki, K., Nagahama, M., *et al.* (2004) Involvement of BNIP1 in apoptosis and endoplasmic reticulum membrane fusion. *EMBO J.* **23**, 3216–3226
78. Singh, S. B., Tandon, R., Krishnamurthy, G., Vikram, R., Sharma, N., Basu, S. K., *et al.* (2003) Rab5-mediated endosome–endosome fusion regulates hemoglobin endocytosis in Leishmania donovani. *EMBO J.* **22**, 5712
79. Ansari, I., Basak, R., and Mukhopadhyay, A. (2022) Hemoglobin endocytosis and intracellular trafficking: a novel way of heme acquisition by Leishmania. *Pathogens* **11**, 585
80. Fernandes, A. C. S., Soares, D. C., Neves, R. F. C., Koeller, C. M., Heise, N., Adade, C. M., *et al.* (2020) Endocytosis and exocytosis in Leishmania amazonensis are modulated by bromoenol lactone. *Front. Cell Infect. Microbiol.* **10**, 39
81. Thompson, J. D., Higgins, D. G., and Gibson, T. J. (1994) Clustal W: improving the sensitivity of progressive multiple sequence alignment through sequence weighting, position-specific gap penalties and weight matrix choice. *Nucleic Acids Res.* **22**, 4673–4680
82. Waterhouse, A. M., Procter, J. B., Martin, D. M. A., Clamp, M., and Barton, G. J. (2009) Jalview Version 2—a multiple sequence alignment editor and analysis workbench. *Bioinformatics* **25**, 1189–1191
83. Zhang, Y. (2008) I-TASSER server for protein 3D structure prediction. *BMC Bioinformatics* **9**, 40
84. Delano, W. L. (2002) *The PyMOL Molecular Graphics System*, DeLano Scientific LLC, Palo Alto, CA
85. Prasad, V., Kumar, S. S., and Dey, C. S. (2000) Resistance to arsenite modulates levels of α-tubulin and sensitivity to paclitaxel in Leishmania donovani. *Parasitol. Res.* **86**, 838–842
86. Jayanarayan, K. G., and Dey, C. S. (2002) Resistance to arsenite modulates expression of beta- and gamma-tubulin and sensitivity to paclitaxel during differentiation of Leishmania donovani. *Parasitol. Res.* **88**, 754–759
87. Ephros, M., Waldman, E., and Zilberstein, D. (1997) Pentostam induces resistance to antimony and the preservative chlorocresol in Leishmania donovani promastigotes and axenically grown amastigotes. *Antimicrob. Agents Chemother.* **41**, 1064–1068
88. Ha, D. S., Schwarz, J. K., Turco, S. J., and Beverley, S. M. (1996) Use of the green fluorescent protein as a marker in transfected Leishmania. *Mol. Biochem. Parasitol.* **77**, 57–64
89. Kolaskar, A. S., and Tongaonkar, P. C. (1990) A semi-empirical method for prediction of antigenic determinants on protein antigens. *FEBS Lett.* **276**, 172–174
90. Jha, P. K., Khan, M. I., Mishra, A., Das, P., and Sinha, K. K. (2017) HAT2 mediates histone H4K4 acetylation and affects micrococcal nuclease sensitivity of chromatin in Leishmania donovani. *PLoS One* **12**, e0177372
91. Kapler, G. M., Coburn, C. M., and Beverley, S. M. (1990) Stable transfection of the human parasite Leishmania major delineates a 30-kilobase region sufficient for extrachromosomal replication and expression. *Mol. Cell Biol.* **10**, 1084–1094
92. Smith, P. K., Krohn, R. I., Hermanson, G. T., Mallia, A. K., Gartner, F. H., Provenzano, M. D., *et al.* (1985) Measurement of protein using bicinchoninic acid. *Anal. Biochem.* **150**, 76–85
93. Kumar, N., and Dey, C. S. (2002) Metformin enhances insulin signalling in insulin-dependent and-independent pathways in insulin resistant muscle cells. *Br. J. Pharmacol.* **137**, 329–336
94. Arastu-Kapur, S., Ford, E., Ullman, B., and Carter, N. S. (2003) Functional analysis of an inosine-guanosine transporter from Leishmania donovani. The role of conserved residues, aspartate 389 and arginine 393. *J. Biol. Chem.* **278**, 33327–33333
95. Denny, P. W., Gokool, S., Russell, D. G., Field, M. C., and Smith, D. F. (2000) Acylation-dependent protein export in Leishmania. *J. Biol. Chem.* **275**, 11017–11025
96. Barak, B., Williams, A., Bielopolski, N., Gottfried, I., Okun, E., Brown, M. A., *et al.* (2010) Tomosyn expression pattern in the mouse Hippocampus suggests both presynaptic and postsynaptic functions. *Front. Neuroanat.* **4**, 149
97. O'Toole, E., Greenan, G., Lange, K. I., Srayko, M., and Müller-Reichert, T. (2012) The role of γ-tubulin in centrosomal microtubule organization. *PLoS One* **7**, e29795
98. Kuras, Z., Kucher, V., Gordon, S. M., Neumeier, L., Chimote, A. A., Filipovich, A. H., *et al.* (2012) Modulation of KV1.3 channels by protein kinase A I in T lymphocytes is mediated by the disc large 1-tyrosine kinase Lck complex. *Am. J. Physiol. Cell Physiol.* **302**, C1504–C1512

99. Rueden, C. T., Schindelin, J., Hiner, M. C., DeZonia, B. E., Walter, A. E., Arena, E. T., *et al.* (2017) ImageJ2: ImageJ for the next generation of scientific image data. *BMC Bioinformatics* **18**, 529
100. Sharma, M., and Dey, C. S. (2021) Role of Akt isoforms in neuronal insulin signaling and resistance. *Cell Mol. Life Sci.* **78**, 7873–7898
101. Sharma, M., and Dey, C. S. (2022) PHLPP isoforms differentially regulate Akt isoforms and AS160 affecting neuronal insulin signaling and insulin resistance *via* Scribble. *Cell Commun. Signal.* **20**, 179
102. Tamura, K., Stecher, G., and Kumar, S. (2021) MEGA11: molecular evolutionary genetics analysis version 11. *Mol. Biol. Evol.* **38**, 3022–3027